Am J Physiol Heart Circ Physiol 305: H1761–H1771, 2013.
First published October 4, 2013; doi:10.1152/ajpheart.00159.2013.

Inhibition of NF-κB activation by a novel IKK inhibitor reduces the severity of experimental autoimmune myocarditis via suppression of T-cell activation

Ryo Watanabe,[1] Ryoko Wakizono Azuma,[2] Jun-ichi Suzuki,[3] Masahito Ogawa,[3] Akiko Itai,[4] Yasunobu Hirata,[3] Issei Komuro,[5] and Mitsuaki Isobe[1]

[1]*Department of Cardiovascular Medicine, Tokyo Medical and Dental University, Yushima, Bunkyo, Tokyo, Japan;* [2]*Department of Clinical Laboratory, Tokyo Medical and Dental University, Yushima, Bunkyo, Tokyo, Japan;* [3]*Department of Advanced Clinical Science and Therapeutics, University of Tokyo, Hongo, Bunkyo, Tokyo, Japan;* [4]*Institute of Medicinal Molecular Design, Hongo, Bunkyo-ku, Tokyo, Japan; and* [5]*Department of Cardiovascular Medicine, University of Tokyo, Hongo, Bunkyo, Tokyo, Japan*

Submitted 25 February 2013; accepted in final form 22 September 2013

Watanabe R, Azuma RW, Suzuki J, Ogawa M, Itai A, Hirata Y, Komuro I, Isobe M. Inhibition of NF-κB activation by a novel IKK inhibitor reduces the severity of experimental autoimmune myocarditis via suppression of T-cell activation. *Am J Physiol Heart Circ Physiol* 305: H1761–H1771, 2013. First published October 4, 2013; doi:10.1152/ajpheart.00159.2013.—NF-κB, which is activated by the inhibitor of NF-κB kinase (IKK), is involved in the progression of inflammatory disease. However, the effect of IKK inhibition on the progression of myocarditis is unknown. We examined the effect of IKK inhibition on the progression of myocarditis. Lewis rats were immunized with porcine cardiac myosin to induce experimental autoimmune myocarditis (EAM). We administered the IKK inhibitor (IMD-0354; 15 mg·kg^{-1}·day^{-1}) or vehicle to EAM rats daily. Hearts were harvested 21 days after immunization. Although the untreated EAM group showed increased heart weight-to-body weight ratio, and severe myocardial damage, these changes were attenuated in the IKK inhibitor-treated group. Moreover, IKK inhibitor administration significantly reduced NF-κB activation and mRNA expression of IFN-γ, IL-2, and monocyte chemoattractant protein-1 in myocardium compared with vehicle administration. In vitro study showed that the IKK inhibitor treatment inhibited T-cell proliferation and Th1 cytokines production induced by myosin stimulation. The IKK inhibitor ameliorated EAM by suppressing inflammatory reactions via suppression of T-cell activation.

myocarditis; inflammation; NF-κB kinase

ACUTE MYOCARDITIS IS A SERIOUS disease in humans; patients with myocarditis may suffer from rapidly progressive heart failure, shock, or severe arrhythmia. Although acute myocardial inflammation is an essential etiology for its progression, no effective treatment has been elucidated (3, 13, 30, 49). Because autoimmunity is important in myocarditis, a reaction to cardiac myosin may contribute to the development (14). In the pathology of myocarditis, T cells activated by antigen infiltrate into the myocardium, which may lead to myocardial damage by inflammatory reaction to myosin (23). Subsequently, the infiltration of CD4-positive T cells and macrophages into the myocardium promotes inflammatory reactions in the myocardium by releasing Th1 cytokines (e.g., IFN-γ and IL-2) (7) and chemokines [e.g., monocyte chemoattractant protein (MCP)-1] (11). NF-κB, which is regulated by NF-κB kinase (IKK), induces expression of genes that participate in the progression of inflammation (29, 41). Previously, we examined the effect of decoy oligonucleotide against NF-κB on ventricular remodeling after myocarditis (47). This report showed that NF-κB activity increased markedly in experimental autoimmune myocarditis (EAM) rat myocardium and that NF-κB is a key regulator in the progression of EAM. Activation of NF-κB induces gene programs that lead to transactivation of factors including Th1 cytokines and chemokines, promoting the inflammatory status involved in myocarditis (12, 16, 20, 38). Because NF-κB is the main factor in the development of inflammation, inhibition of its activation may be an effective therapy for myocarditis from the standpoint of preventing inflammation.

Recently, we developed IMD-0354, a novel inhibitor of IKK (19, 34, 41). This drug is a selective IKK-β inhibitor, blocks IκBα phosphorylation, and prevents NF-κB p65 nuclear translocation. Some previous studies reported the beneficial effects of IMD-0354 and its prodrug on inflammation-related cardiovascular diseases (15, 34, 35, 42). Therefore, regulation of NF-κB activation by the IKK inhibitor might have a potent effect on the treatment of myocarditis. However, the effect of IKK inhibitor treatment on the progression of myocarditis is unknown. Thus we assessed the hypothesis that IKK inhibitor treatment attenuates cardiac inflammation in the progression of myocarditis. EAM in a rat model is characterized by severe myocardial damage and multinucleated giant cell infiltration. This has been used as a disease model for human acute giant cell myocarditis (8). We examined the effect of IKK inhibition on EAM.

METHODS

Induction of EAM. Male Lewis rats (6-wk-old; body weights 150 to 200 g) were purchased from Charles River Laboratories Japan. They were fed a standard diet and water and were maintained in compliance with animal welfare guidelines of the Institute of Experimental Animals, Tokyo Medical and Dental University. Also, protocols were approved by the Institutional Animal Care and Use Committee of the Tokyo Medical and Dental University. Purified porcine cardiac myosin (Sigma Chemical, St. Louis, MO) was emulsified with an equal volume of complete Freund's adjuvant (Difco, Sparks, MD) supplemented with *Mycobacterium tuberculosis* H37RA (Disco) at a concentration of 10 mg/ml. On *day 0*, rats were injected in the footpads subcutaneously with 0.2 ml of emulsion, yielding an immunizing dose of 1.0 mg/body of cardiac myosin per rat (9) anesthetized by intraperitoneal administration of pentobarbital sodium (25 mg/kg; Dainihon Chemical, Osaka, Japan). We also used unimmunized (normal)

Address for reprint requests and other correspondence: J.-i. Suzuki, Dept. of Advanced Clinical Science and Therapeutics, Graduate School of Medicine, Univ. of Tokyo, 7-3-1 Hongo, Bunkyo-ku, Tokyo 113-8655, Japan (e-mail: junichisuzuki-circ@umin.ac.jp).

rats parallel with the diseased protocol. Unimmunized rats were injected saline instead of emulsion of myosin on *day 0*.

IKK inhibitor administration. The IKK inhibitor IMD-0354 was provided by the Institute of Medicinal Molecular Design. The drug was dissolved in 0.5% carboxy methyl cellulose (CMC) solution immediately before use. In the EAM phase, cardiac inflammation starts on approximately *day 14*, and the peak of inflammation is expected to occur on *day 21* (25). For this reason, we administered the IKK inhibitor either from *day 1* or from *day 14*, and harvested hearts and spleens on *day 21*. Rats were assigned randomly to five groups: *1*) daily CMC intraperitoneal injection to normal rats from *day 1* to *day 20* [normal + vehicle group; $n = 6$], *2*) daily IMD-0354 intraperitoneal injection (15 $mg \cdot kg^{-1} \cdot day^{-1}$) to normal rats from *day 1* to *day 20* [normal + IKKi(1–20); $n = 5$], *3*) daily CMC intraperitoneal injection to EAM rats from *day 1* to *day 20* [EAM + vehicle; $n = 18$], *4*) daily IMD-0354 intraperitoneal injection (15 $mg \cdot kg^{-1} \cdot day^{-1}$) to EAM rats from *day 1* to *day 20* [EAM + IKKi(1–20); $n = 13$], and *5*) daily IMD-0354 intraperitoneal injection (15 $mg \cdot kg^{-1} \cdot day^{-1}$) to EAM rats from *day 14* to *day 20* [EAM + IKKi(14–20); $n = 10$]. Administration dose of the IKK inhibitor was calculated from that of previous articles (17, 19, 31, 34, 35).

Echocardiogram. Transthoracic echocardiography was performed on animals anesthetized by intraperitoneal administration of pentobarbital sodium (25 mg/kg) on *day 21*. An echocardiography machine with a 7.5-MHz transducer (Nemio; Toshiba, Tokyo, Japan) was used for M-mode left ventricular (LV) echocardiographic recording. A two-dimensional targeted M-mode echocardiogram was obtained along the short-axis view of the LV papillary muscles (40). LV posterior wall thickness at diastole (LVPWd), interventricular septal thickness at diastole (IVSTd), and percent ejection fraction (EF) were calculated from the M-mode recordings.

Histopathological examination. Hearts and spleens were harvested immediately after all rats were killed by the cutting of the abdominal aorta under anesthesia after the echocardiographic examination on *day 21*. After heart weights were measured, hearts were divided into apex, midventricular, and basal level slices. Apex level slice was frozen by liquid nitrogen, and it was stored at −80°C until before use. This slice was used as the sample for Western blotting or real-time RT-PCR. Midventricular level slices and spleens were fixed by formalin or embedded by optimum cutting temperature compound (Sakura Finetek, Tokyo, Japan). OCT compound-embedded slices were frozen by liquid nitrogen. These slices were used for histopathological or immunohistochemical examination. Formaldehyde-fixed paraffin sections were stained with hematoxylin and eosin or the Mallory method. The extent of inflammatory cell infiltration and myocardial necrosis was estimated using hematoxylin and eosin staining. The degree of fibrosis was estimated using Mallory staining. The cell infiltration area ratio (cell infiltration area/total area expressed as a percentage) and the fibrosis area ratio (the Mallory stained area/total area expressed as a percentage) were calculated by a computer-assisted analyzer (Scion Image beta 4.0.2) as described previously (1, 9, 28).

Immunohistochemistry. Immunohistochemistry was performed to detect CD4- or CD8-positive T cells, macrophages, NF-κB p65, and phospho-NF-κB p65 in the heart or the spleen on *day 21*. Paraffin or frozen sections were incubated with primary antibodies against CD4 (10B5; Abcam, Cambridge, UK), CD8 (OX8; BD PharMingen California), CD68 (as a marker of macrophage; ED1; Santa Cruz Biotechnology, Santa Cruz, CA), and NF-κB p65 (Abcam) for 8 h at 4°C and washed in PBS followed by biotinylated secondary antibodies (Nichirei, Tokyo, Japan) at 5 mg/ml for 30 min at room temperature. Finally, each section was reacted with AEC (aminoethylcarbazole complex) solution (Nichirei) for 5 to 30 min. Sections were counterstained with hematoxylin solution. We counted the number of positive cells against CD4, CD8, and CD68 in randomly selected five random microscopical fields (original magnification, ×200) per sample section, and averaged it (10). Immunofluorescence double staining was performed to identify colocalization of CD4 positive cells and phospho-NF-κB p65 in the heart and spleen. Antibodies against CD4 (OX35; mouse- monoclonal; Abcam) and phospho-NF-κB p65 (Ser536; 93H1; rabbit- monoclonal; Cell Signaling Technology) were co-incubated and detected with Alexa 488 anti-mouse antibody (Life Technologies Japan) and Alexa 568 anti-rabbit antibody (Life Technologies), respectively. Nuclei were stained with 4′,6-diamidino-2-phenylindole.

Extraction of proteins from hearts. To extract tissue protein, frozen cardiac tissues from an apex level heart slice was homogenized in lysis buffer of 50 mM Tris·HCl (pH 7.5), 150 mM NaCl, 1% Triton X-100, 2 mM EGTA, 10 mM EDTA, 100 nM NaF containing protease inhibitor cocktail tablets (Roche Diagnostic, Basel, Switzerland) and phosphatase inhibitor cocktail tablets (Roche Diagnostic). Nuclear and cytosolic proteins were isolated from frozen cardiac tissues from the same apex level heart slice using Nuclear Extraction Kit (Epigentek Group). Protein concentrations were measured with a BCA protein assay (Bio-Rad, Milan, Italy) to equalize the protein concentrations of all samples. Protein samples were stored at −80°C until they were used.

Western blotting. Equal amounts of proteins were separated by SDS-PAGE, transferred to a nitrocellulose membrane, and incubated overnight with antibodies to IκB (Abcam), phospho-IκB (Cell Signaling Technology), GAPDH (Cell Signaling Technology), NF-κB p65 (Abcam), phospho-NF-κB p65 (Ser536; Cell Signaling Technology), and Lamin A/C (Cell Signaling Technology) at 4°C. The membranes were incubated with a secondary antibody (Amersham Biosciences, Piscataway, NJ) for 2 h and developed with ECL reagent (Amersham Biosciences). Enhanced chemiluminescence was detected with an LAS-1000 (Fujifilm, Tokyo, Japan). The value was calculated using ImageJ [National Institutes of Health (NIH)].

Real-time RT-PCR. Total RNA was isolated from frozen apex level heart slice tissues using TRIsure (Bioline, London, UK), and cDNA was prepared with the high capacity cDNA Reverse Transcription Kit (Applied Biosystems). Real-time PCR in a Step One real-time PCR system (Applied Biosystems) was used to determine the mRNA expression of IFN-γ (Assay ID: Rn99999014_m1), IL-2 (Assay ID: Rn00587673_m1), and MCP-1 (Assay ID: Rn00580555_m1) and 18s rRNA (Assay ID: Hs99999901_s1) as a control. cDNA was run in duplicates, quantitative data were calculated using the comparative

Table 1. *Echocardiographic parameters*

	n	LV Diameter at Diastole, mm	LV Diameter at Systole, mm	Ejection Fraction, %	Interventricular Septal Thickness at Diastole, mm	LV Posterior Wall Thickness at Diastole, mm
Normal + vehicle	6	6.3 ± 0.26	3.0 ± 0.17	89 ± 0.5	1.8 ± 0.16	2.2 ± 0.22
Normal + IKKi(1–20)	5	6.5 ± 0.21	3.4 ± 0.09	85 ± 1.4	1.6 ± 0.09	2.1 ± 0.35
EAM + vehicle	11	6.0 ± 0.28	3.6 ± 0.33	75 ± 4.7	2.5 ± 0.20#	2.9 ± 0.29
EAM + IKKi(1–20)	12	6.6 ± 0.15	4.0 ± 0.27	76 ± 3.9	1.7 ± 0.11*	1.9 ± 0.12*
EAM + IKKi(14–20)	7	6.1 ± 0.11	3.8 ± 0.16	74 ± 2.2	1.6 ± 0.09*	2.5 ± 0.14

Values are means ± SE. Early IKK inhibitor treatment [experimental autoimmune myocarditis (EAM) + IKKi(1–20)] suppressed an increase of interventricular septal thickness at diastole and left ventricular (LV) posterior wall thickness at diastole values, whereas late IKK inhibitor treatment [EAM + IKKi (14–20)] only suppressed an increase of interventricular septal thickness at diastole value compared with vehicle treatment [EAM + vehicle] on *day 21*. #$P < 0.05$ vs. normal + vehicle; *$P < 0.05$ vs. EAM + vehicle.

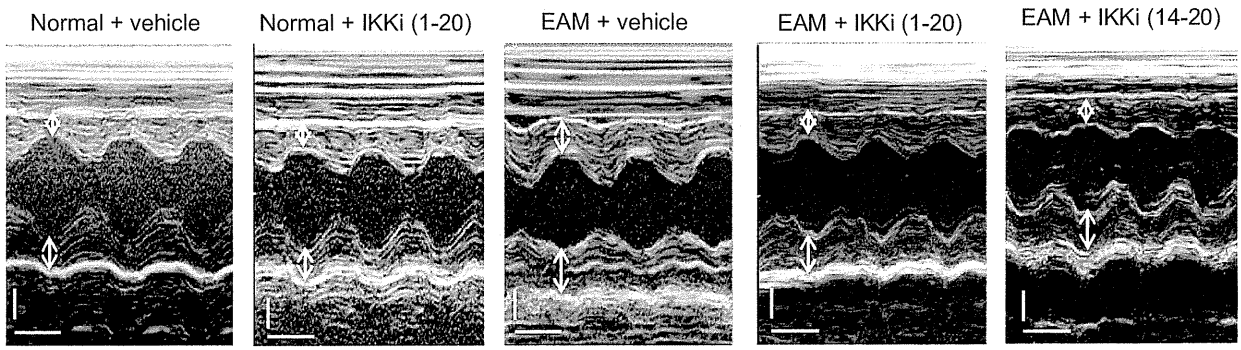

Fig. 1. Representative M-mode echocardiograms on *day 21*. Arrows indicate anterior and posterior walls of left ventricle. Scale bars: 2 millimeter (vertical) and 0.1 s (horizontal).

CT ($\Delta\Delta C_T$) method, and the mRNA expression was normalized by normal rat hearts (28, 32).

T-cell proliferation assay. Cells were isolated from spleen in the EAM + vehicle group on *day 21*. Cells (5×10^6/well) were cultured in 96-well culture plates with 50 μg/ml purified porcine heart myosin. The IKK inhibitor was added to each well at various concentrations. In vitro dosage of the IKK inhibitor was determined according to that in previous articles (34, 35). Cultures were incubated at 37°C under 5% CO_2 for 3 days. Cells were centrifuged at 1,200 rpm for 5 min, and the supernatants were stored at −80°C until before use. T-cell proliferation was assessed with the Cell Counting Kit-8 (Dojindo, Tokyo, Japan) with the use of cells of the precipitation. Cell proliferation was expressed as the optical density (9).

Enzyme-linked immunosorbent assay. We performed enzyme-linked immunosorbent assay (ELISA) to examine the production of Th1 cytokines from T cells using the supernatants of cell culture in T-cell proliferation assays. Concentrations of IFN-γ and IL-2 in cell culture supernatant were determined with the Rat IL-2 quantikine ELISA kit (R & D Systems, Minneapolis, MN) and rat IFN-γ ELISA KIT (Gen-Probe, San Diego, CA) according to the manufacturer's instructions.

Statistical analysis. All data are expressed as means ± SE. Statistical analyses were performed with statistical software (Stat View; SAS Institute). Student's *t*-test was used to compare data between the two groups. Data differences between multiple groups were subjected to ANOVA followed by a Bonferroni-Dunn test. Differences were considered statistically significant at a value of $P < 0.05$.

RESULTS

Echocardiographic parameters. On *day 21*, the values of LV diameter at diastole, LV diameter at systole, and EF did not show any statistical difference among all groups. Regarding IVSTd and LVPWd values, no significant difference was observed between the normal + vehicle group and the normal + IKKi(1–20) group. IVSTd values significantly increased in the EAM + vehicle group compared with the normal + vehicle group. IVSTd and LVPWd values in the EAM + IKKi(1–20) group were reduced compared with those of the EAM + vehicle group. Additionally, IVSTd value was reduced in the EAM + IKKi(14–20) group compared with that of the EAM + vehicle group, although LVPWd value was not changed. There was no significant difference regarding IVSTd and LVPWd values between the EAM + IKKi(14–20) group and the EAM + IKKi(1–20) group (Table 1 and Fig. 1).

The IKK inhibitor suppressed heart weight gain by cardiac inflammation. The normal + IKKi(1–20) group did not show any change in heart weight compared with the normal + vehicle group. The EAM + vehicle group hearts demonstrated an increase of the heart-to-body weight ratio compared with that of the normal + vehicle group. This ratio in the EAM + IKKi(1–20) group was significantly smaller than that of the EAM + vehicle group, whereas the EAM + IKKi(14–20) group was not statistically different compared with the EAM + vehicle group. There was no significant difference of this ratio between the EAM + IKKi(14–20) group and the EAM + IKKi(1–20) group (Fig. 2).

The IKK inhibitor reduced myocardial damage characterized by cell infiltration and fibrosis in EAM. Histopathologically, the heart of the EAM + vehicle group showed severe myocarditis lesions that were composed of extensive inflammatory cell infiltration and myocardial fibrosis on *day 21*. However, the cell infiltration area ratios in the EAM + IKKi(1–20) group (12.9 ± 3.6%; $P < 0.05$) and the EAM + IKKi(14–20) group (22.5 ± 2.9%; $P < 0.05$) were significantly fewer than those in the EAM + vehicle group (36.5 ± 3.4%) (Fig. 3, *A–C*). Similarly, the fibrosis area ratios in the EAM + IKKi(1–20) group (15.8 ± 4.0%; $P < 0.05$) and the EAM + IKKi(14–20) group (21.4 ±

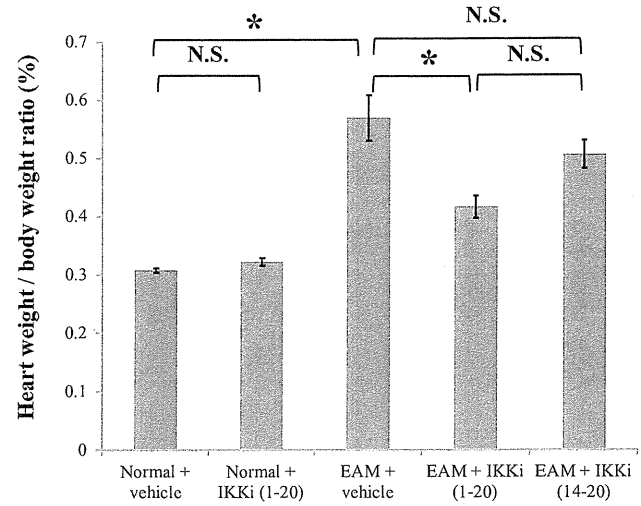

Fig. 2. Heart-to-body weight ratio. The experimental autoimmune myocarditis (EAM) + IKKi(1–20) group had a smaller the heart-to-body weight ratio than the EAM + vehicle group. The EAM + IKKi(14–20) group did not show the effect of the heart-to-body weight ratio compared with that of the EAM + vehicle group on *day 21* [normal + vehicle, $n = 5$; normal + IKKi(1–20), $n = 5$; EAM + vehicle, $n = 12$; EAM + IKKi(1–20), $n = 12$; EAM + IKKi(14–20), $n = 10$]. *$P < 0.05$. NS, not significant.

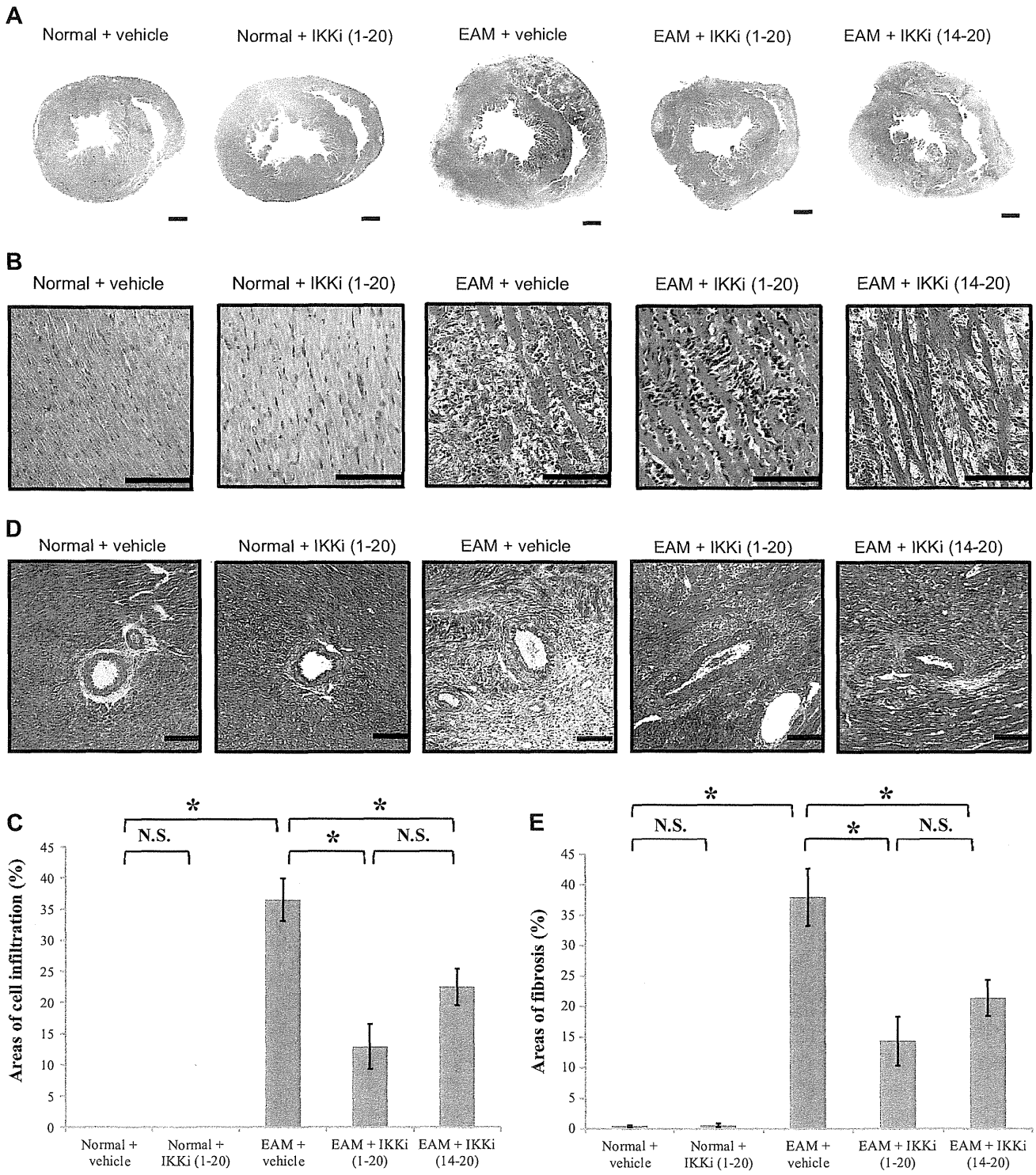

Fig. 3. Histopathological findings. Representative low-power (magnification, ×10; scale bars = 1 millimeter; *A*) and high-power (magnification, ×400; scale bars = 100 μm; *B*) photomicrographs of hematoxylin and eosin-stained cross-sections are shown. *C*: quantitative data of cell infiltration area. IKK inhibitor treatment significantly suppressed cell infiltration into myocardium on *day 21* [normal + vehicle, $n = 5$; normal + IKKi(1–20), $n = 5$; EAM + vehicle, $n = 14$; EAM + IKKi(1–20), $n = 12$; EAM + IKKi(14–20), $n = 10$]. $^*P < 0.05$. *D*: representative photomicrographs (magnification, ×200; scale bars = 100 μm) of Mallory-stained cross-sections. *E*: quantitative data of fibrosis area. IKK inhibitor treatment significantly suppressed cardiac fibrosis on *day 21* [normal + vehicle, $n = 5$; normal + IKKi(1–20), $n = 5$; EAM + vehicle, $n = 14$; EAM + IKKi(1–20), $n = 12$; EAM + IKKi(14–20), $n = 10$]. $^*P < 0.05$.

2.9%; $P < 0.05$) were significantly lower than those in the EAM + vehicle group (37.9 ± 4.7%), respectively (Fig. 3, *D* and *E*). There was no significant difference regarding these histopathological changes between the EAM + IKKi(1–20) group and the EAM + IKKi(14–20) group. Hearts from the normal + IKKi(1–20) group did not show abnormal histopathological change compared with the normal + vehicle group.

The IKK inhibitor attenuated inflammatory cell infiltration in EAM hearts. After histopathological examination, we analyzed the effect of IKK inhibitor treatment on each inflammatory infiltrating cell. Hearts from the EAM + vehicle group showed massive infiltrations of CD-4 positive T cells and CD68-positive macrophages, and moderate infiltration of CD8-positive T cells on *day 21*. However, the EAM + IKKi(1–20) group showed significant reductions of CD4-, CD8-, and CD68-positive cell numbers compared with the EAM + vehicle group (Fig. 4, *A–D*).

Localization of NF-κB activation in EAM. To investigate NF-κB activity in EAM, we performed immunohistochemical analysis. On *day 21*, NF-κB p65 was expressed in the cytoplasm of cardiac tissues from the normal + vehicle group. In contrast, strong expression of NF-κB p65 was observed mainly in the nucleus of the infiltrating cells in the myocardium as shown by arrows in the hearts from the EAM + vehicle group (Fig. 5*A*). On this occasion, NF-κB p65 phosphorylation (as a marker of NF-κB activation) was detected in CD4-positive T cells that infiltrated the myocardium in the EAM + vehicle group (Fig. 5*B*). CD4-positive T cells play a critical role in the development of EAM. The spleen is a major source of immune cells, including CD4-positive T cells. Immune cells derived from the spleen migrate to the inflammatory affected area through the blood stream (37). Hence, we examined NF-κB activation in the spleen during the development of EAM. In the spleen obtained from the EAM + vehicle group, we observed enhanced colocalization of phospho-NF-κB p65 and CD4-positive T cells compared with that of the normal + vehicle group (Fig. 5*C*).

IKK inhibitor suppressed NF-κB activation in EAM hearts. To examine the effect of IKK inhibitor treatment on NF-κB activity in the heart of EAM, we analyzed nuclear NF-κB p65 protein expression, NF-κB p65 phosphorylation level, and cytosolic phospho-IκB-to-IκB ratio (35). The EAM + vehicle group showed enhanced nuclear NF-κB p65 protein expression compared with the normal + vehicle group. However, nuclear NF-κB p65 protein expression was significantly reduced in the EAM + IKKi(1–20) group compared with the EAM + vehicle group on *day 21* (Fig. 6, *A* and *B*). Phosphorylation level of NF-κB p65 (as shown by phospho-NF-κB-to-total NF-κB ratio) was reduced by IKK inhibitor administration (Fig. 6, *C* and *D*). Moreover, the level of cytosolic phospho-IκBα-to-IκB

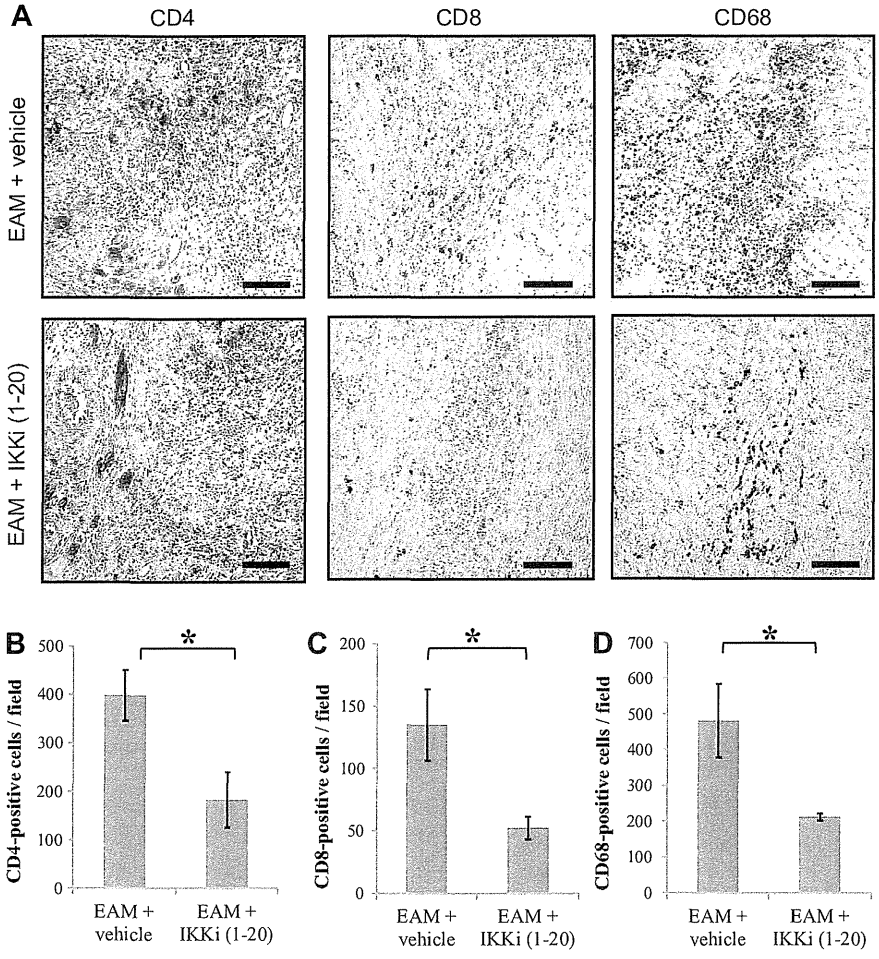

Fig. 4. Infiltrations of inflammation-related cells on *day 21*. *A*: representative CD4 staining, CD8 staining, and CD68 staining photomicrographs (magnification, ×200; scale bars = 100 μm). Quantitative results of immunohistochemistry for CD4-positive T cell [EAM + vehicle, $n = 8$; EAM + IKKi(1–20), $n = 7$; *B*], CD8-positive T cell [EAM + vehicle, $n = 7$; EAM + IKKi(1–20), $n = 8$; *C*], and CD68-positive macrophage [EAM + vehicle, $n = 7$; EAM + IKKi(1–20), $n = 6$; *D*] are shown. IKK inhibitor treatment reduced numbers of CD4-, CD8-, and CD68-positive infiltrating cells in EAM hearts on *day 21*. *$P < 0.05$.

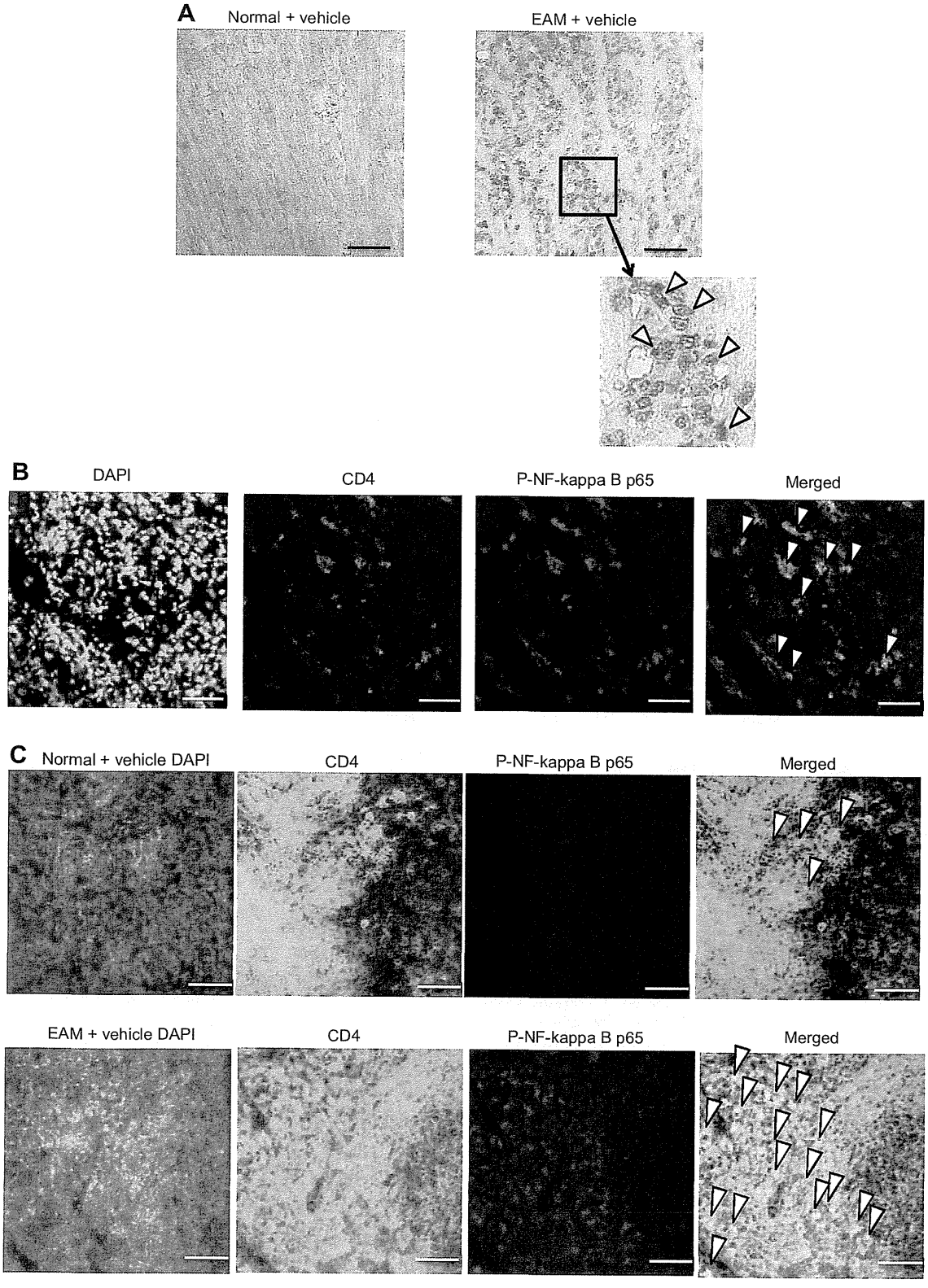
A
Normal + vehicle
EAM + vehicle
B
DAPI
CD4
P-NF-kappa B p65
Merged
C
Normal + vehicle DAPI
CD4
P-NF-kappa B p65
Merged
EAM + vehicle DAPI
CD4
P-NF-kappa B p65
Merged

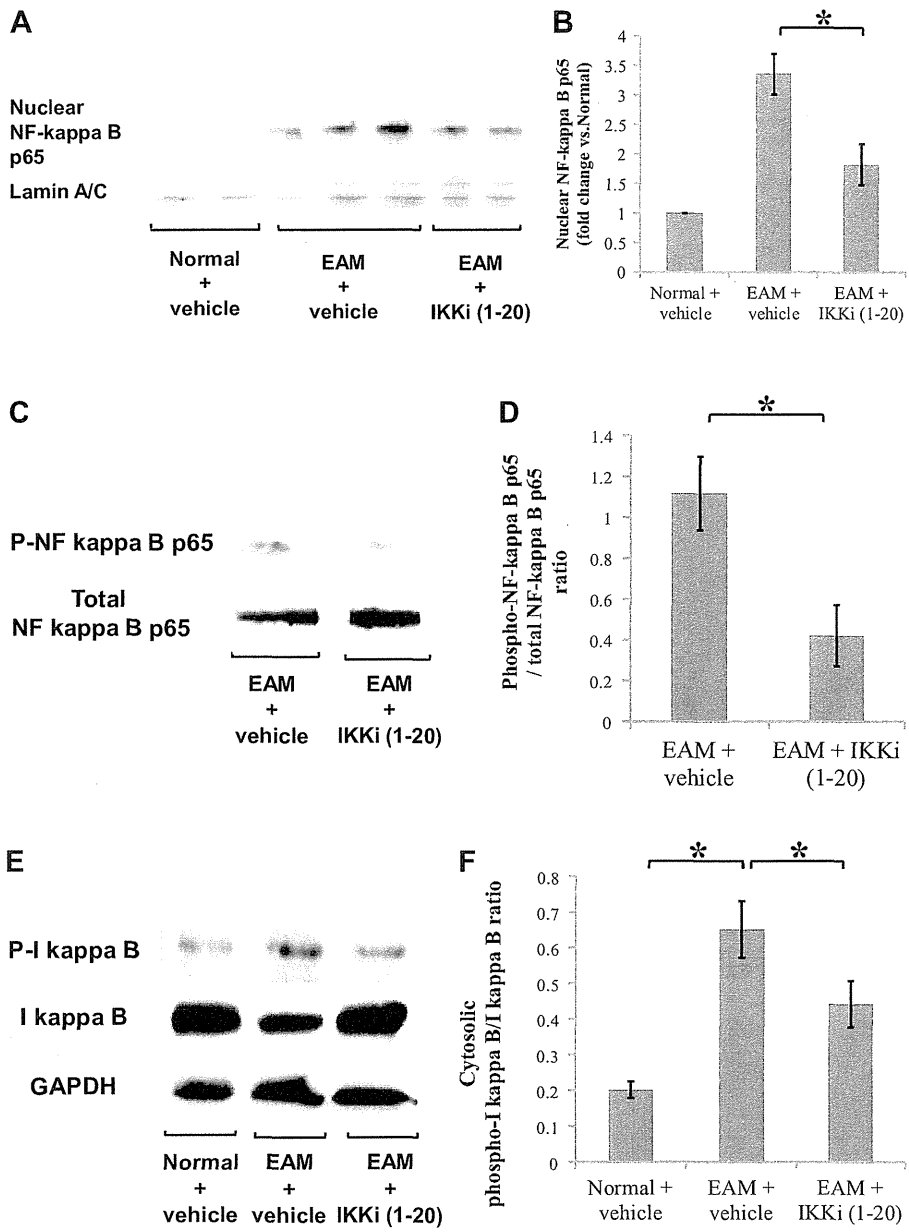

Fig. 6. Activity of NF-κB in each group on *day 21*. *A*: results of representative Western blotting for nuclear NF-κB p65 and lamin A/C. *B*: relative quantitative results of NF-κB p65 nuclear translocation [normal + vehicle, $n = 3$; EAM + vehicle, $n = 5$; EAM + IKKi(1–20), $n = 4$]. *C*: results of representative Western blotting for phospho-NF-κB p65 and total-NF-κB p65. *D*: quantitative results of phospho-NF-κB p65-to-total-NF-κB p65 ratio (as an index of NF-κB p65 phosphorylation) [EAM + vehicle, $n = 4$; EAM + IKKi(1–20), $n = 4$]. *E*: results of representative Western blotting for cytosolic IκBα, phospho-IκBα, and GAPDH. *F*: quantitative results of cytosolic phospho-IκBα-to-IκBα ratio (as an index of IκBα phosphorylation) [normal + vehicle, $n = 6$; EAM + vehicle, $n = 11$; EAM + IKKi(1–20), $n = 8$]. IKK inhibitor administration suppressed NF-κB activation in EAM hearts tissue. $^*P < 0.05$.

ratio in EAM hearts increased in the EAM + vehicle group compared with the normal + vehicle group. However, it decreased by IKK inhibitor administration (Fig. 6, *E* and *F*).

Altered inflammation-related gene expression by IKK inhibition in EAM hearts. Th1 cytokines and chemokines are known to promote myocardial inflammation during EAM (7, 11). Therefore, we examined the effect of IKK inhibitor treatment on mRNA expression of a chemokine and Th1 cytokines in hearts on *day 21* using real-time RT-PCR. In the EAM + vehicle group, mRNA expressions of IFN-γ, IL-2, and MCP-1 were enhanced compared with the normal + vehicle group. However, mRNA expressions of these genes were significantly suppressed in the EAM +

Fig. 5. Localization of NF-κB activation in EAM on *day 21*. *A*: representative immunohistochemistry of hearts from the normal + vehicle group and the EAM + vehicle group (magnification, ×400; scale bars = 50 μm). In EAM hearts (EAM + vehicle), NF-κB p65 was expressed in the nucleus of infiltrating cells (as shown by arrows). *B*: representative immunofluorescence double staining findings of the myocardium in the EAM + vehicle group on *day 21* (magnification, ×400; scale bars = 50 μm). Phospho (P)-NF-κB p65 was detected on CD4-positive infiltrating cells (as shown by arrows) in the EAM + vehicle group. *C*: representative immunofluorescence double staining findings of the spleen from the normal + vehicle group and the EAM + vehicle group on *day 21* (magnification, ×400; scale bars = 50 μm). Colocalization of phospho-NF-κB p65 and CD4-positive cells (as shown by arrows) were observed in the spleens from the EAM + vehicle group. DAPI, 4′,6-diamidino-2-phenylindole.

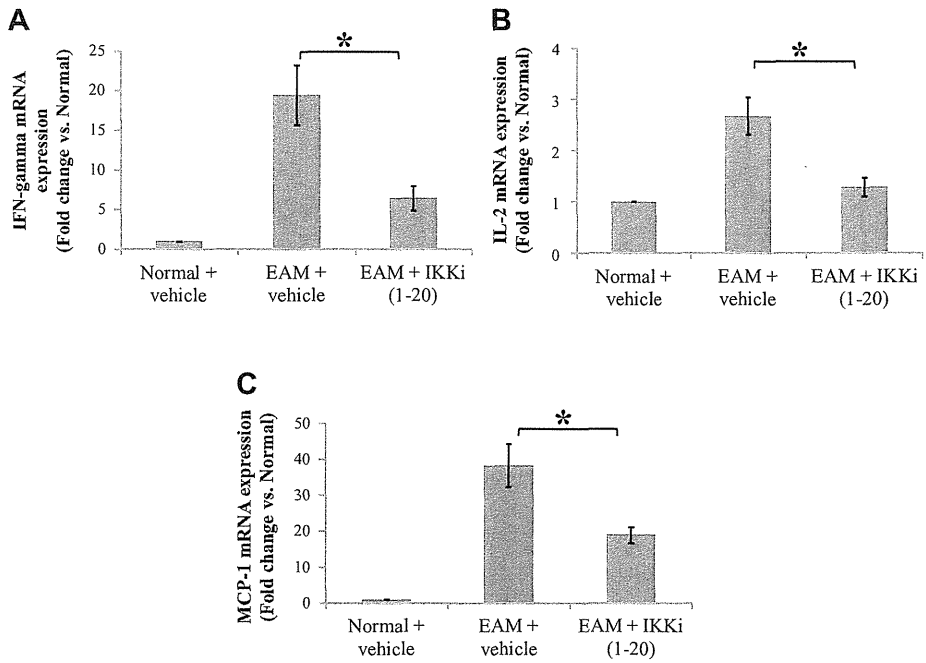

Fig. 7. mRNA expression of inflammation-related genes. Results of real-time RT-PCR for IFN-γ (*A*), IL-2 (*B*), and monocyte chemoattractant protein (MCP-1; *C*). IKK inhibitor treatment significantly suppressed mRNA expressions of IFN-γ, IL-2, and MCP-1 on *day 21* [normal + vehicle, $n = 3$; EAM + vehicle, $n = 12$; EAM + IKKi(1–20), $n = 9$]. *$P < 0.05$.

IKKi(1–20) group compared with the EAM + vehicle group (Fig. 7, *A–C*).

Suppression of antigen-induced T-cell proliferation by IKK inhibitor treatment. Our present study revealed that NF-κB activation was observed in CD4-positive T cells in the heart and spleen during the development of EAM. Additionally, previous studies reported that EAM is transferable to other individuals via T cells derived from the spleen of EAM (21, 46). T cells activated by antigen mediate the development of EAM. Therefore, we performed a T-cell proliferation assay to examine the effect of IKK inhibitor on antigen-induced T-cell proliferation using splenocytes of EAM. As a result, T-cell proliferation was significantly increased by myosin restimulation. IKK inhibitor treatment suppressed myosin-induced T-cell proliferation in a dose-dependent manner (Fig. 8).

Effect of IKK inhibitor on the production of Th1 cytokines in vitro. It is known that Th1 cytokines released from CD4-positive T cells mediate the progression of EAM (33). Thus, to examine the effects of IKK inhibitor on the production of Th1 cytokines from T cells activated by antigen, we performed ELISA using supernatants collected from T-cell proliferation assays. In consequence, productions of IFN-γ and IL-2 were significantly increased by myosin restimulation. However, IKK inhibitor treatment suppressed the production of these th1 cytokines in a dose-dependent manner (Fig. 9, *A* and *B*).

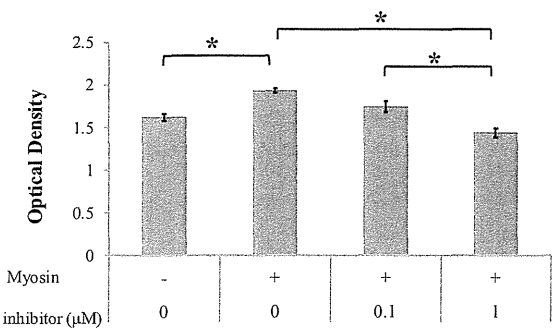

Fig. 8. The effect of IKK inhibitor treatment on antigen-induced T-cell proliferation. The IKK inhibitor suppressed antigen-induced T-cell proliferation in a dose-dependent manner ($n = 10$ each). *$P < 0.05$.

DISCUSSION

NF-κB is a key factor for the progression of inflammation (35, 47). Our previous articles showed that inhibition of NF-κB activation by the IKK inhibitor significantly suppressed pro-inflammatory mediators in myocardial ischemia model (34, 45). Inflammation is an essential pathological feature of acute myocarditis. Although the effectiveness of the IKK inhibitor on cardiac diseases associated with inflammation was shown, the effect of the IKK inhibitor on myocarditis remains unknown.

IKK inhibitor treatment did not change the value of EF compared with vehicle treatment on *day 21*. However, the EAM + IKKi(1–20) group exhibited an antihypertrophic effect, as shown by suppression of increases of LVPWd and IVSTd values. This effect was consistent with the result that IKK inhibitor treatment suppressed heart weight gain. The increased wall thickness is considered to be owing to interstitial edema associated with progression of myocardial inflammation. In contrast, the EAM + IKKi(14–20) group suppressed the increase of IVSTd value; however, it did not affect LVPWd value and heart weight gain. Earlier IKK inhibitor treatment may be more effective. The severity of histological myocardial damage characterized by cell infiltration and fibrosis was significantly reduced in both the EAM + IKKi(14–20) group and the EAM + IKKi(1–20) group compared with the EAM + vehicle group. Additionally, it should be noted that there was no significant difference regarding this effect between the EAM + IKKi(14–20) group and the EAM +

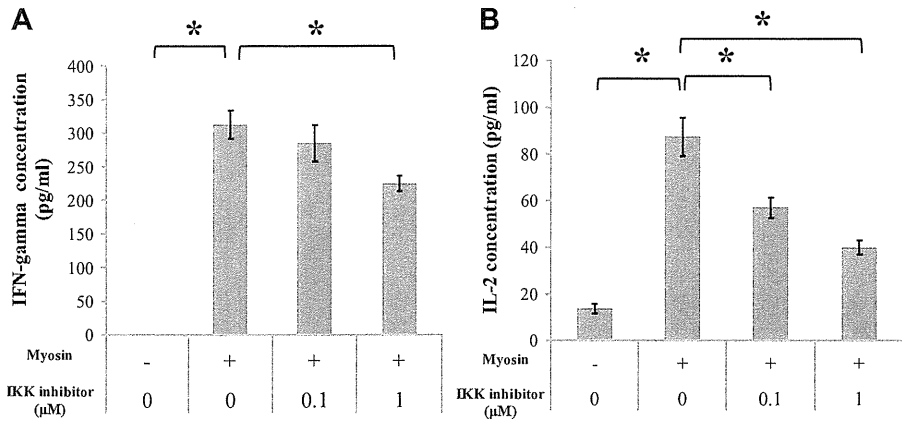

Fig. 9. The effect of IKK inhibitor treatment on antigen-induced production of Th1 cytokines. Results of enzyme-linked immunosorbent assay for IFN-γ (*A*) and IL-2 (*B*) are shown. The production of Th1-type cytokines, including IFN-γ (n = 10 each) and IL-2 (n = 10 each), was significantly reduced by IKK inhibitor administration in vitro. *$P < 0.05$.

IKKi(1–20) group. We revealed that even when IKK inhibitor administration began from *day 14*, IKK inhibitor treatment suppressed myocardial damage and it was not inferior to the early IKK inhibitor treatment group [EAM + IKKi(1–20)]. Thus our results suggest that the treatment effect of IMD-0354 was due to the suppression of the inflammatory reaction that was caused around *day 14*. In a clinical setting, time lag occurs before patients are diagnosed with myocarditis and receive medical treatment. Therefore, IKK inhibitor treatment from *day 14* to *day 21* [EAM + IKKi(14–20)] was a trial to inspect utility as a therapeutic medicine of myocarditis. Meanwhile, there was no significant difference in echocardiographic parameters and histopathological findings between the normal + vehicle group and the normal + IKKi(1–20) group. These results suggest that the IKK inhibitor IMD-0354 does not affect normal hearts.

We observed massive infiltrations of CD4-positive T cells and CD68-positive macrophages, and moderate infiltration of CD8-positive T cells in the EAM + vehicle group hearts tissue. Infiltration cells into myocardium consist of mainly macrophages and CD4-positive T cells in EAM, and this result is consistent with those of previous studies (14, 22). These inflammatory cell infiltrations were suppressed by IKK inhibitor administration. NF-κB induces activation of inflammatory cells such as T cells and macrophages (2, 18). During the inflammatory phase of EAM, Th1 cytokines are enhanced and they mediate interaction between CD4-positive T cells and macrophages, which lead to cardiac damages (8, 14, 33). In particular, CD4-positive T cells proliferate oneself by releasing IL-2 and activate macrophages by releasing IFN-γ. Subsequently, activating macrophages damage myocardium (33). MCP-1 is known as a chemotactic factor and plays essential role in the inflammatory reaction involved in the progress of myocarditis by having an influence on the recruitment of inflammatory cells (11). Many inflammation-related genes including IFN-γ, IL-2, and MCP-1 are expressed by NF-κB (5, 43, 44), and its suppression prevents the development of EAM (11, 27, 36). Our in vivo studies revealed that mRNA expression of IFN-γ, IL-2, and MCP-1 were suppressed by IKK inhibitor treatment through inhibition of NF-κB activation in EAM heart tissues. Therefore, inhibition of NF-κB activation by IKK inhibitor treatment to suppress expression of inflammation-related genes may prevent harmful inflammatory cell infiltration in myocarditis.

In the process of EAM, CD4-positive T cells were activated by cardiac myosin and then recruited to the target organ (heart) (39). It is known that this cell play a particularly significant role in the pathophysiology of EAM. We demonstrated that NF-κB activation was observed mainly in CD4-positive T cells infiltrating the myocardium in EAM. A major source of inflammatory cells, including CD4-positive T cells, is the spleen (37). Therefore, we examined NF-κB activity in CD4-positive T cells of the spleen during EAM. We also detected NF-κB activation of CD4-positive T cells in spleens in EAM. A recent study reported that immune cells derived from the spleen reach the myocardium via the blood stream and induced inflammatory reaction during inflammation-related cardiac disease (24). Moreover, some previous studies reported that splenocytes play a role of the pathogen and transferred myocarditis (21, 26, 46). Therefore, we investigated the direct effects of the IKK inhibitor on T cells, which were activated by antigen and derived from the spleen. Our in vitro study revealed that IKK inhibitor treatment suppressed myosin induced T-cell proliferation and production of Th1 cytokines. NF-κB activation is necessary for T-cell activation, differentiation, and proliferation (4). Activated T cells secrete various cytokines and chemokines via NF-κB activation, which activate other inflammatory cells or cardiomyocytes in the myocardium and cause further recruitment of inflammatory cells (34, 48). Antigen-induced T-cell proliferation and subsequent production of Th1 cytokines from T cells are an essential response for the development of EAM (8). This evidence demonstrates that the IKK inhibitor suppressed the activation of T cells and attenuated the development of EAM. Therefore, our results suggested that IMD-0354 attenuated the severity of EAM by targeting NF-κB of T cells during the inflammatory phase in EAM.

The present study showed for the first time that the IKK inhibitor IMD-0354 reduces the severity of EAM. This effect is associated with the reduction of inflammatory-related gene expression by inhibition of NF-κB activation. Some previous studies reported that administration of pharmacological agents indirectly inhibited NF-κB activation and suppressed the progression of EAM (1, 14, 40). Therefore, the IKK inhibitor IMD-0354, which directly inhibits NF-κB activation, may be promising as a therapeutic drug for the treatment of myocarditis. It is noteworthy that the IKK inhibitor will be clinically available in the near future. IMD-1041, which is a prodrug of IMD-0354, also inhibits IKK-β in vivo and in vitro (6).

Because this compound is an investigational drug, it is not yet on the market. To prove the clinical effect of IMD-1041, we started an interventional, randomized, placebo control and double blind clinical trial. Thus the IKK inhibitor will be used to treat myocarditis and other cardiovascular diseases in clinical settings in the future. Our data clearly indicate that IKK is critical for EAM development and its inhibition has significant effects for treating myocardial inflammation. In conclusion, IKK regulation is promising in the treatment of clinical acute myocarditis.

ACKNOWLEDGMENTS

We thank Noriko Tamura and Yasuko Matsuda for excellent technical assistance.

GRANTS

This study was supported by Takeda Science Foundation, Suzuken Memorial Foundation, a grant from the Research Foundation for Pharmaceutical Sciences, and the Japan Society for the Promotion of Science through its Funding Program for World-Leading Innovative R & D on Science and Technology (FIRST Program).

DISCLOSURES

No conflicts of interest, financial or otherwise, are declared by the author(s).

AUTHOR CONTRIBUTIONS

Author contributions: R.W., R.W.A., J.-i.S., and A.I. conception and design of research; R.W. and R.W.A. performed experiments; R.W. and R.W.A. analyzed data; R.W., R.W.A., J.-i.S., M.O., and M.I. interpreted results of experiments; R.W. prepared figures; R.W. drafted manuscript; R.W., J.-i.S., M.O., and M.I. edited and revised manuscript; R.W., J.-i.S., M.O., A.I., Y.H., I.K., and M.I. approved final version of manuscript.

REFERENCES

1. **Azuma RW, Suzuki J, Ogawa M, Futamatsu H, Koga N, Onai Y, Kosuge H, Isobe M.** HMG-CoA reductase inhibitor attenuates experimental autoimmune myocarditis through inhibition of T cell activation. *Cardiovasc Res* 64: 412–420, 2004.
2. **Barnes PJ, Karin M.** Nuclear factor-kappaB: a pivotal transcription factor in chronic inflammatory diseases. *N Engl J Med* 336: 1066–1071, 1997.
3. **Batra AS, Lewis AB.** Acute myocarditis. *Curr Opin Pediatr* 13: 234–239, 2001.
4. **Brechmann M, Mock T, Nickles D, Kiessling M, Weit N, Breuer R, Muller W, Wabnitz G, Frey F, Nicolay JP, Booken N, Samstag Y, Klemke CD, Herling M, Boutros M, Krammer PH, Arnold R.** A PP4 holoenzyme balances physiological and oncogenic nuclear factor-kappa B signaling in T lymphocytes. *Immunity* 37: 697–708, 2012.
5. **Corn RA, Aronica MA, Zhang F, Tong Y, Stanley SA, Kim SR, Stephenson L, Enerson B, McCarthy S, Mora A, Boothby M.** T cell-intrinsic requirement for NF-kappa B induction in postdifferentiation IFN-gamma production and clonal expansion in a Th1 response. *J Immunol* 171: 1816–1824, 2003.
6. **Fukuda S, Horimai C, Harada K, Wakamatsu T, Fukasawa H, Muto S, Itai A, Hayashi M.** Aldosterone-induced kidney injury is mediated by NF-κB activation. *Clin Exp Nephrol* 15: 41–49, 2011.
7. **Fuse K, Kodama M, Aizawa Y, Yamaura M, Tanabe Y, Takahashi K, Sakai K, Miida T, Oda H, Higuma N.** Th1/Th2 balance alteration in the clinical course of a patient with acute viral myocarditis. *Jpn Circ J* 65: 1082–1084, 2001.
8. **Fuse K, Kodama M, Ito M, Okura Y, Kato K, Hanawa H, Aoki S, Aizawa Y.** Polarity of helper T cell subsets represents disease nature and clinical course of experimental autoimmune myocarditis in rats. *Clin Exp Immunol* 134: 403–408, 2003.
9. **Futamatsu H, Suzuki J, Kosuge H, Yokoseki O, Kamada M, Ito H, Inobe M, Isobe M, Uede T.** Attenuation of experimental autoimmune myocarditis by blocking activated T cells through inducible costimulatory molecule pathway. *Cardiovasc Res* 59: 95–104, 2003.
10. **Futamatsu H, Suzuki J, Mizuno S, Koga N, Adachi S, Kosuge H, Maejima Y, Hirao K, Nakamura T, Isobe M.** Hepatocyte growth factor ameliorates the progression of experimental autoimmune myocarditis: a potential role for induction of T helper 2 cytokines. *Circ Res* 96: 823–830, 2005.
11. **Goser S, Ottl R, Brodner A, Dengler TJ, Torzewski J, Egashira K, Rose NR, Katus HA, Kaya Z.** Critical role for monocyte chemoattractant protein-1 and macrophage inflammatory protein-1alpha in induction of experimental autoimmune myocarditis and effective anti-monocyte chemoattractant protein-1 gene therapy. *Circulation* 112: 3400–3407, 2005.
12. **Granelli-Piperno A, Nolan P.** Nuclear transcription factors that bind to elements of the IL-2 promoter. Induction requirements in primary human T cells. *J Immunol* 147: 2734–2739, 1991.
13. **Haas GJ.** Etiology, evaluation, and management of acute myocarditis. *Cardiol Rev* 9: 88–95, 2001.
14. **Haga T, Suzuki J, Kosuge H, Ogawa M, Saiki H, Haraguchi G, Maejima Y, Isobe M, Uede T.** Attenuation of experimental autoimmune myocarditis by blocking T cell activation through 4–1BB pathway. *J Mol Cell Cardiol* 46: 719–727, 2009.
15. **Hamaya R, Ogawa M, Kobayashi N, Suzuki J, Itai A, Hirata Y, Nagai R, Isobe M.** A novel IKK inhibitor prevents progression of restenosis after arterial injury in mice. *Int Heart J* 53: 133–138, 2012.
16. **Hernandez-Presa M, Bustos C, Ortego M, Tunon J, Renedo G, Ruiz-Ortega M, Egido J.** Angiotensin-converting enzyme inhibition prevents arterial nuclear factor-kappa B activation, monocyte chemoattractant protein-1 expression, and macrophage infiltration in a rabbit model of early accelerated atherosclerosis. *Circulation* 95: 1532–1541, 1997.
17. **Inayama M, Nishioka Y, Azuma M, Muto S, Aono Y, Makino H, Tani K, Uehara H, Izumi K, Itai A, Sone S.** A novel IκB kinase-beta inhibitor ameliorates bleomycin-induced pulmonary fibrosis in mice. *Am J Respir Crit Care Med* 173: 1016–1022, 2006.
18. **Ivashkiv LB.** Inflammatory signaling in macrophages: transitions from acute to tolerant and alternative activation states. *Eur J Immunol* 41: 2477–2481, 2011.
19. **Kamon J, Yamauchi T, Muto S, Takekawa S, Ito Y, Hada Y, Ogawa W, Itai A, Kasuga M, Tobe K, Kadowaki T.** A novel IKKbeta inhibitor stimulates adiponectin levels and ameliorates obesity-linked insulin resistance. *Biochem Biophys Res Commun* 323: 242–248, 2004.
20. **Kang H, Moon JY, Sohn NW.** Regulation of interferon-gamma, interleukin-4 and interleukin-2 by Schizonepeta tenuifolia through differential effects on nuclear factor-kappaB, NFATc2 and STAT4/6. *Exp Biol Med (Maywood)* 235: 230–236, 2010.
21. **Kodama M, Matsumoto Y, Fujiwara M.** In vivo lymphocyte-mediated myocardial injuries demonstrated by adoptive transfer of experimental autoimmune myocarditis. *Circulation* 85: 1918–1926, 1992.
22. **Kodama M, Zhang S, Hanawa H, Shibata A.** Immunohistochemical characterization of infiltrating mononuclear cells in the rat heart with experimental autoimmune giant cell myocarditis. *Clin Exp Immunol* 90: 330–335, 1992.
23. **Leuschner F, Katus HA, Kaya Z.** Autoimmune myocarditis: past, present and future. *J Autoimmun* 33: 282–289, 2009.
24. **Leuschner F, Panizzi P, Chico-Calero I, Lee WW, Ueno T, Cortez-Retamozo V, Waterman P, Gorbatov R, Marinelli B, Iwamoto Y, Chudnovskiy A, Figueiredo JL, Sosnovik DE, Pittet MJ, Swirski FK, Weissleder R, Nahrendorf M.** Angiotensin-converting enzyme inhibition prevents the release of monocytes from their splenic reservoir in mice with myocardial infarction. *Circ Res* 107: 1364–1373, 2010.
25. **Liu W, Li WM, Gao C, Sun NL.** Effects of atorvastatin on the Th1/Th2 polarization of ongoing experimental autoimmune myocarditis in Lewis rats. *J Autoimmun* 25: 258–263, 2005.
26. **Maisel A, Cesario D, Baird S, Rehman J, Haghighi P, Carter S.** Experimental autoimmune myocarditis produced by adoptive transfer of splenocytes after myocardial infarction. *Circ Res* 82: 458–463, 1998.
27. **Matsui Y, Inobe M, Okamoto H, Chiba S, Shimizu T, Kitabatake A, Uede T.** Blockade of T cell costimulatory signals using adenovirus vectors prevents both the induction and the progression of experimental autoimmune myocarditis. *J Mol Cell Cardiol* 34: 279–295, 2002.
28. **Ngoc PB, Suzuki J, Ogawa M, Hishikari K, Takayama K, Hirata Y, Nagai R, Isobe M.** The anti-inflammatory mechanism of prostaglandin e2 receptor 4 activation in rat experimental autoimmune myocarditis. *J Cardiovasc Pharmacol* 57: 365–372, 2011.

29. **Niederberger E, Geisslinger G.** The IKK-NF-kappaB pathway: a source for novel molecular drug targets in pain therapy? *FASEB J* 22: 3432–3442, 2008.
30. **Oakley CM.** Myocarditis, pericarditis and other pericardial diseases. *Heart* 84: 449–454, 2000.
31. **Ogawa H, Azuma M, Muto S, Nishioka Y, Honjo A, Tezuka T, Uehara H, Izumi K, Itai A, Sone S.** IkappaB kinase beta inhibitor IMD-0354 suppresses airway remodelling in a Dermatophagoides pteronyssinus-sensitized mouse model of chronic asthma. *Clin Exp Allergy* 41: 104–115, 2011.
32. **Ogawa M, Suzuki J, Takayama K, Senbonmatsu T, Hirata Y, Nagai R, Isobe M.** Impaired post-infarction cardiac remodeling in chronic kidney disease is due to excessive renin release. *Lab Invest* 92: 1766–1776, 2012.
33. **Okura Y, Yamamoto T, Goto S, Inomata T, Hirono S, Hanawa H, Feng L, Wilson CB, Kihara I, Izumi T, Shibata A, Aizawa Y, Seki S, Abo T.** Characterization of cytokine and iNOS mRNA expression in situ during the course of experimental autoimmune myocarditis in rats. *J Mol Cell Cardiol* 29: 491–502, 1997.
34. **Onai Y, Suzuki J, Kakuta T, Maejima Y, Haraguchi G, Fukasawa H, Muto S, Itai A, Isobe M.** Inhibition of IkappaB phosphorylation in cardiomyocytes attenuates myocardial ischemia/reperfusion injury. *Cardiovasc Res* 63: 51–59, 2004.
35. **Onai Y, Suzuki J, Maejima Y, Haraguchi G, Muto S, Itai A, Isobe M.** Inhibition of NF-κB improves left ventricular remodeling and cardiac dysfunction after myocardial infarction. *Am J Physiol Heart Circ Physiol* 292: H530–H538, 2007.
36. **Perez Leiros C, Goren N, Sterin-Borda L, Borda ES.** Myocardial dysfunction in an experimental model of autoimmune myocarditis: role of IFN-γ. *Neuroimmunomodulation* 4: 91–97, 1997.
37. **Savvatis K, van Linthout S, Miteva K, Pappritz K, Westermann D, Schefold JC, Fusch G, Weithauser A, Rauch U, Becher PM, Klingel K, Ringe J, Kurtz A, Schultheiss HP, Tschope C.** Mesenchymal stromal cells but not cardiac fibroblasts exert beneficial systemic immunomodulatory effects in experimental myocarditis. *PLos One* 7: e41047, 2012.
38. **Sica A, Dorman L, Viggiano V, Cippitelli M, Ghosh P, Rice N, Young HA.** Interaction of NF-kappaB and NFAT with the interferon-gamma promoter. *J Biol Chem* 272: 30412–30420, 1997.
39. **Smith SC, Allen PM.** Myosin-induced acute myocarditis is a T cell-mediated disease. *J Immunol* 147: 2141–2147, 1991.
40. **Suzuki J, Ogawa M, Futamatsu H, Kosuge H, Sagesaka YM, Isobe M.** Tea catechins improve left ventricular dysfunction, suppress myocardial inflammation and fibrosis, and alter cytokine expression in rat autoimmune myocarditis. *Eur J Heart Fail* 9: 152–159, 2007.
41. **Suzuki J, Ogawa M, Muto S, Itai A, Isobe M, Hirata Y, Nagai R.** Novel IkB kinase inhibitors for treatment of nuclear factor-kB-related diseases. *Expert Opin Investig Drugs* 20: 395–405, 2011.
42. **Tanaka T, Ogawa M, Suzuki J, Sekinishi A, Itai A, Hirata Y, Nagai R, Isobe M.** Inhibition of IκB phosphorylation prevents load-induced cardiac dysfunction in mice. *Am J Physiol Heart Circ Physiol* 303: H1435–H1445, 2012.
43. **Ueda A, Okuda K, Ohno S, Shirai A, Igarashi T, Matsunaga K, Fukushima J, Kawamoto S, Ishigatsubo Y, Okubo T.** NF-kappa B and Sp1 regulate transcription of the human monocyte chemoattractant protein-1 gene. *J Immunol* 153: 2052–2063, 1994.
44. **Verweij CL, Geerts M, Aarden LA.** Activation of interleukin-2 gene transcription via the T-cell surface molecule CD28 is mediated through an NF-κB-like response element. *J Biol Chem* 266: 14179–14182, 1991.
45. **Wakatsuki S, Suzuki J, Ogawa M, Masumura M, Muto S, Shimizu T, Takayama K, Itai A, Isobe M.** A novel IKK inhibitor suppresses heart failure and chronic remodeling after myocardial ischemia via MMP alteration. *Expert Opin Ther Targets* 12: 1469–1476, 2008.
46. **Wu JL, Matsui S, Zong ZP, Nishikawa K, Sun BG, Katsuda S, Fu M.** Amelioration of myocarditis by statin through inhibiting cross-talk between antigen presenting cells and lymphocytes in rats. *J Mol Cell Cardiol* 44: 1023–1031, 2008.
47. **Yokoseki O, Suzuki J, Kitabayashi H, Watanabe N, Wada Y, Aoki M, Morishita R, Kaneda Y, Ogihara T, Futamatsu H, Kobayashi Y, Isobe M.** cis Element decoy against nuclear factor-kappaB attenuates development of experimental autoimmune myocarditis in rats. *Circ Res* 89: 899–906, 2001.
48. **Yoshida T, Hanawa H, Toba K, Watanabe H, Watanabe R, Yoshida K, Abe S, Kato K, Kodama M, Aizawa Y.** Expression of immunological molecules by cardiomyocytes and inflammatory and interstitial cells in rat autoimmune myocarditis. *Cardiovasc Res* 68: 278–288, 2005.
49. **Zee-Cheng CS, Tsai CC, Palmer DC, Codd JE, Pennington DG, Williams GA.** High incidence of myocarditis by endomyocardial biopsy in patients with idiopathic congestive cardiomyopathy. *J Am Coll Cardiol* 3: 63–70, 1984.

ELSEVIER

Brain & Development 36 (2014) 180–182

BRAIN & DEVELOPMENT
Official Journal of the Japanese Society of Child Neurology

www.elsevier.com/locate/braindev

Case report

MELAS phenotype associated with m.3302A>G mutation in mitochondrial tRNA$^{Leu(UUR)}$ gene

Masahide Goto [a], Hirofumi Komaki [a,*], Takashi Saito [a], Yoshiaki Saito [a], Eiji Nakagawa [a], Kenji Sugai [a], Masayuki Sasaki [a], Ichizo Nishino [b], Yu-ichi Goto [c]

[a] *Department of Child Neurology, National Center Hospital, National Center of Neurology and Psychiatry, Tokyo, Japan*
[b] *Department of Neuromuscular Research, National Institute of Neuroscience, National Center of Neurology and Psychiatry, Tokyo, Japan*
[c] *Department of Mental Retardation and Birth Defect Research, National Institute of Neuroscience, National Center of Neurology and Psychiatry, Tokyo, Japan*

Received 26 March 2012; received in revised form 31 January 2013; accepted 13 March 2013

Abstract

The m.3302A>G mutation in the mitochondrial tRNA$^{Leu(UUR)}$ gene has been identified in only 12 patients from 6 families, all manifesting adult-onset slowly progressive myopathy with minor central nervous system involvement. An 11-year-old boy presented with progressive proximal-dominant muscle weakness from age 7 years. At age 10, he developed recurrent stroke-like episodes. Mitochondrial myopathy, encephalopathy, lactic acidosis, plus stroke-like episodes (MELAS) was diagnosed by clinical symptoms and muscle biopsy findings. Mitochondrial gene analysis revealed a heteroplasmic m.3302A>G mutation. Histological examination showed strongly SDH reactive blood vessels (SSVs), not present in previous cases with myopathies due to the m.3302A>G mutation. These findings broaden the phenotypic spectrum of this mutation.

Keywords: MELAS; Myopathy; m.3302A>G mutation

1. Introduction

The m.3302A>G mutation in the mitochondrial tRNA$^{Leu(UUR)}$ gene was identified in 6 families including 12 patients with adult-onset slowly progressive myopathy and minor central nervous system complications including hearing disabilities and oculomotor symptoms [1–4]. In contrast, we experienced a child harboring the same mutation who showed the mitochondrial encephalopathy, lactic acidosis, plus stroke-like episodes (MELAS) phenotype. Approximately 80% of MELAS cases are caused by an A-to-G transition mutation at position 3243 in the mitochondrial tRNA$^{Leu(UUR)}$ (MTTL1) gene [5]. The relationship of this mutation to the MELAS phenotype is noteworthy.

2. Case report

A 7-year-old boy presented with gait disturbance and progressive proximal-dominant muscle weakness. He had normal psychomotor development until the development of the symptoms. His maternal members including his mother did not have symptoms associated with mitochondrial diseases such as short stature, diabetes mellitus, hearing loss, mental retardation, and cardiac complication. Generalized seizures emerged at age 10 years, subsequently occurring 8 times within one year. Electroencephalography revealed sporadic sharp

* Corresponding author. Address: Department of Child Neurology, National Center Hospital, National Center of Neurology and Psychiatry (NCNP), 4-1-1 Ogawahigashi-cho, Kodaira, Tokyo 187-8551, Japan. Tel.: +81 42 341 2711; fax: +81 42 344 6745.
E-mail address: komakih@ncnp.go.jp (H. Komaki).

0387-7604/$ - see front matter © 2013 The Japanese Society of Child Neurology. Published by Elsevier B.V. All rights reserved.
http://dx.doi.org/10.1016/j.braindev.2013.03.001

Table 1
Laboratory data.

Serum		(Normal range)	
Creatine kinase	716	(57–197)	IU/L
Lactate	68.4	(3.0–17.0)	mg/dL
Pyruvate	1.60	(0.3–0.94)	mg/dL
Cerebrospinal fluid			
Lactate	44.0	(8.4–16.6)	mg/dL
Pyruvate	1.92	(0.63–1.27)	mg/dL

waves at mid-frontal areas. On physical examination at age 11 years, he showed winged scapulas and proximal muscle weakness necessitated Gowers' maneuver to stand. His deep tendon reflexes were decreased. Cranial nerve findings were unremarkable. IQ testing (WISC-III) revealed borderline mental retardation (full IQ 76). Serum creatine kinase, lactate and pyruvate, as well as cerebrospinal lactate and pyruvate, were elevated (Table 1).

Histological examination of biopsied muscle showed 30% of muscle to be ragged-red fibers (RRFs) by modified Gomori-trichrome staining. Succinate dehydrogenase (SDH) staining revealed strongly SDH reactive blood vessels (SSVs). Cytochrome c oxidase (COX) staining demonstrated variable enzyme activities from strongly positive to negative. Both RRFs and SSVs showed variable COX activities.

Respiratory chain enzyme activities in biopsied tissues were measured using previously reported methods [6]. The ratio of muscle complex I/II activities was markedly reduced to 12% of control values. Those of complex III/II and IV/II activities were 43% and 40%, respectively. In myoblasts and fibroblasts, these ratios were all within control ranges (Table 2).

Mitochondrial gene analysis was conducted as described elsewhere [7], and identified the m.3302A>G mutation located within the coding sequence of $tRNA^{Leu(UUR)}$. The heteroplasmy proportion of the m.3302A>G mutation was determined for each tissue by real-time PCR method using Taq-Man® probe on ABI 7700 according to the manufacturer. Mutation loads were 89.5 ± 0.3% in biopsied muscle, 85.8 ± 0.7% in myoblasts, 86.9 ± 0.8% in fibroblasts and 36.1 ± 2.3% in white blood cells.

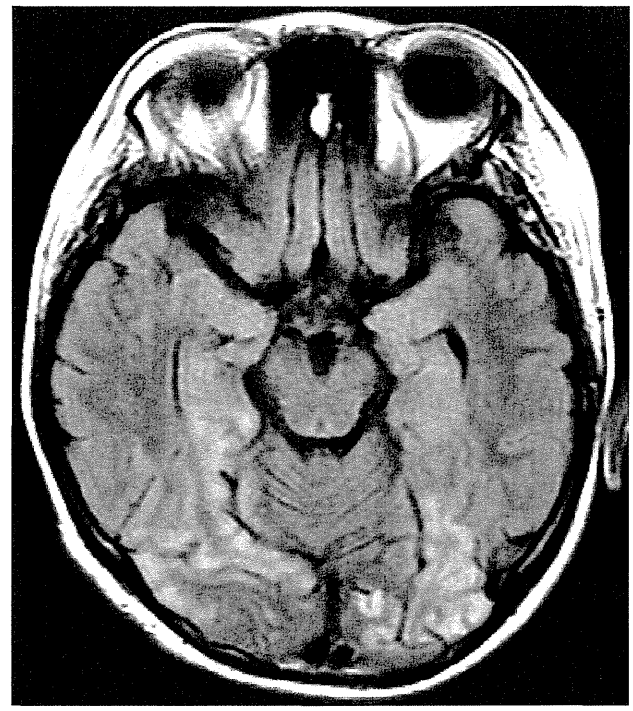

Fig. 1. Brain magnetic resonance imaging of the patient (fluid-attenuated inversion recovery imaging). Bilateral occipital lesions with high signal intensity are noted, whose distribution in not conforming to that of vascular territories.

After MELAS was diagnosed, the patient experienced stroke-like episodes with headache, vomiting, and occasionally cortical blindness. Brain magnetic resonance imaging (MRI) showed bilateral occipital lesions, confined to the cortical ribbon and not conforming to the distribution of vascular territories, with high signal intensity on fluid-attenuated inversion recovery images (Fig. 1). During the follow-up period, repeated MRI examinations never had basal ganglia lesions. At age 12 years, he became wheelchair-bound, and was nocturnal mask-medicated ventilator dependent due to chronic respiratory insufficiency.

Table 2
Respiratory chain enzyme activities.

Complex	Skeletal muscle		Myoblasts		Fibroblasts	
	Patient	Control ($n = 5$)	Patient	Control ($n = 5$)	Patient	Control ($n = 4$)
I/II	0.09	0.26–1.2	3.2	1.3–5.6	2	1.6–3.4
	12%	(0.76 ± 0.39)		(3.0 ± 1.7)		(2.0 ± 0.9)
III/II	0.39	0.72–1.8	3.4	3.2–7.4	5.3	1.9–5.6
	43%	(0.91 ± 0.41)		(4.2 ± 1.6)		(3.5 ± 1.8)
IV/II	0.35	0.42–1.3	3.7	2.1–9.1	2.8	2.2–5.0
	40%	(0.88 ± 0.36)		(4.7 ± 3.1)		(3.3 ± 1.2)

Complex I, III and IV activities are shown as proportions to that of complex II. Control values are expressed as mean ± standard deviation.

3. Discussion

Our patient initially manifested muscle weakness, developing epilepsy and stroke-like episodes years later. Elevated cerebrospinal lactate and pyruvate and bilateral occipital lesions with high signal intensity on MRI characterize the MELAS phenotype, and an m.3302A>G mutation was identified for the first time. The mutation was in a heteroplasmic state, a common feature of pathogenic mtDNA mutations. The significant tissue-to-tissue variability and inability to quantify the tissue specific mutational burden for the brain make it difficult to determine a prognosis for individuals harboring this mutation. Although the percentage of mutation load in differ little from those of in myoblast and fibroblast, the degree of the enzymatic deficiency in muscle, myoblasts, and fibroblasts are diverse in our patient. The threshold effects of this mutation might be different between muscle, fibroblasts and myoblasts.

However, the proportion of mutated mtDNA was highest in leptomeningeal and cortical blood vessel walls in all brain regions in a patient with severe COX deficiency [8]. Since mitochondrial dysfunction in vessels is assumed to be essential in the pathogenesis of stroke-like episodes in MELAS, such heteroplasmy may have been present in our patient. Moreover, although some cases with adult-onset slowly progressive mitochondrial myopathy with m.3302A>G mutations had hearing loss, recurrent headaches, ptosis, progressive external ophthalmoplegia, and depression [3], muscle biopsy revealed RRFs but no SSVs in these cases. Since SSVs represent an increased proportion of mutant mtDNA in vessel walls and are characteristic of MELAS [9,10], the SSVs in muscle tissue might be linked to the brain lesions through abundant mutated mtDNA in blood vessels in the central nervous system in our patient.

His maternal members including his mother did not have symptoms associated with mitochondrial diseases. It would have been useful that we analyze their heteroplasmic conditions, however, we could not obtain the samples of his maternal members because of the disapproval of providing the samples.

In conclusion, our case suggested the m.3302A>G mutation to cause the clinical MELAS phenotype. We should pay attention to headache, convulsion and other symptoms suggesting MELAS in patients with mitochondrial myopathies, particularly those with SSVs on muscle pathology.

Acknowledgments

This work was partly supported by Research Grant (21A-6) for Nervous and Mental Disorders (YG and EN) and Grants-in-Aid for Research on Intractable Diseases (Mitochondrial Disease) (YG and HK) from the Ministry of Health, Labour and Welfare of Japan. We thank Dr. Yutaka Nonoda, and Dr. Hideyuki Hatakeyama, Dr. Chika Sakai, Ms. Mayuko Kato and Ms. Yoshie Sawano for technical assistance.

References

[1] Bindoff LA, Howell N, Poulton J, McCullough DA, Morten KJ, Lightowlers RN, et al. Abnormal RNA processing associated with a novel tRNA mutation in mitochondrial DNA. A potential disease mechanism. J Biol Chem 1993;268:19559–64.
[2] van den Bosch BJ, de Coo IF, Hendrickx AT, Busch HF, de Jong G, Scholte HR, et al. Increased risk for cardiorespiratory failure associated with the A3302G mutation in the mitochondrial DNA encoded $tRNA^{Leu(UUR)}$ gene. Neuromuscul Disord 2004;14:683–8.
[3] Hutchison WM, Thyagarajan D, Poulton J, Marchington DR, Kirby DM, Manji SS, et al. Clinical and molecular features of encephalomyopathy due to the A3302G mutation in the mitochondrial $tRNA^{Leu(UUR)}$ gene. Arch Neurol 2005;62:1920–3.
[4] Ballhausen D, Guerry F, Hahn D, Schaller A, Nuoffer JM, Bonafé L, et al. Mitochondrial tRNALeu(UUR) mutation m.3302A>G presenting as childhood-onset severe myopathy: threshold determination through segregation study. J Inherit Metab Dis, in press. doi:10.1007/s10545-010-9098-2.
[5] Schaefer AM, McFarland R, Blakcly EI, He L, Whittaker RG, Taylor RW, et al. Prevalence of mitochondrial DNA disease in adults. Ann Neurol 2008;63:35–9.
[6] Trounce LA, Kim YL, Jun AS, Wallace DC. Assessment of mitochondrial oxidative phosphorylation in patient muscle biopsies, lymphoblasts, and transmitochondrial cell lines. In: Attardi GM, Chomyn A, editors. Methods in enzymology, vol. 264. San Diego, USA: Academic Press; 1996. p. 484–509.
[7] Akanuma J, Muraki K, Komaki H, Nonaka I, Goto Y. Two pathogenic point mutations exist in the authentic mitochondrial genome, not in the nuclear pseudogene. J Hum Genet 2000;45:337–41.
[8] Betts J, Jaros E, Perry RH, Schaefer AM, Taylor RW, Abdel-All Z, et al. Molecular neuropathology of MELAS: level of heteroplasmy in individual neurons and evidence of extensive vascular involvement. Neuropathol Appl Neurobiol 2006;32:359–73.
[9] Hasegawa H, Matusoka T, Goto Y, Nonaka I. Strongly succinate dehydrogenase-reactive blood vessels in muscles from patients with mitochondrial myopathy, encephalopathy, lactic acidosis, and stroke-like episodes. Ann Neurol 1991;29:601–5.
[10] Goto Y. Clinical features of MELAS and mitochondrial DNA mutations. Muscle Nerve 1995;3:S107–12.

International Journal of Cardiology 162 (2013) 234–239

Contents lists available at ScienceDirect

International Journal of Cardiology

journal homepage: www.elsevier.com/locate/ijcard

Association between cardiopulmonary exercise and dobutamine stress testing in ambulatory patients with idiopathic dilated cardiomyopathy: A comparison with peak VO_2 and VE/VCO_2 slope

Takahiro Okumura [a], Akihiro Hirashiki [a,*], Sumio Yamada [b], Hidehito Funahashi [a], Satoru Ohshima [a], Yuji Kono [c], Xian Wu Cheng [a], Kyosuke Takeshita [a], Toyoaki Murohara [a]

[a] Department of Cardiology, Nagoya University Graduate School of Medicine, Nagoya, Japan
[b] School of Health Sciences, Nagoya University, Nagoya, Japan
[c] Program in Physical and Occupational Therapy, Nagoya University Graduate School of Medicine, Nagoya, Japan

ARTICLE INFO

Article history:
Received 31 October 2010
Received in revised form 18 February 2011
Accepted 13 May 2011

Keywords:
Cardiomyopathy
Dobutamine
Cardiopulmonary exercise testing

ABSTRACT

Background: Both peak VO_2 and VE/VCO_2 slope are considered to be useful predictors of cardiovascular events. The left ventricular (LV) response to dobutamine stress testing (DST) also provides useful prognostic information. However, the relationship between these variables has not been fully investigated. Therefore, the aim of this study is to investigate the association between myocardial contractile reserve measured by DST and cardiopulmonary exercise testing (CPX) variables in patients with idiopathic dilated cardiomyopathy (IDCM).

Methods: Thirty-eight patients were subjected to CPX as well as cardiac catheterization for measurement of LV pressure. The maximum first derivative of LV pressure (LV dP/dt_{max}) was measured at baseline and during dobutamine infusion at incremental doses of 5, 10, and 15 $\mu g\ kg^{-1}\ min^{-1}$. LV dP/dt_{max} at baseline and the percentage increase in LV dP/dt_{max} (ΔLV dP/dt_{max}) induced by DST served as indices of LV contractility and myocardial contractile reserve, respectively.

Results: Peak VO_2, and VE/VCO_2 slope were 18.6 mL $kg^{-1}\ min^{-1}$ and 32.3, respectively. Peak VO_2 was not correlated with LV dP/dt_{max} at baseline. However, peak VO_2 was significantly correlated with ΔLV dP/dt_{max}, and the correlation became more pronounced as the dose of dobutamine was increased. There was no correlation between VE/VCO_2 slope and ΔLV dP/dt_{max}. Multivariate regression analysis revealed that ΔLV dP/dt_{max} was independently correlated with peak VO_2 ($p=0.011$).

Conclusions: Peak VO_2, but not VE/VCO_2 slope, may reflect myocardial contractile reserve in ambulatory patients with IDCM. This study population is small, and therefore large confirmatory studies are needed.

1. Introduction

Heart failure (HF), a major and growing public health problem, appears to result not only from cardiac overload or injury but also from a complex interplay among genetic, neurohormonal, and biochemical changes acting on cardiac myocytes, the cardiac interstitium, or both [1]. Exercise tolerance reflects a number of prognostically important factors, including cardiac function, oxygen-carrying capacity, and autonomic nervous system balance [2–4]. Cardiopulmonary exercise testing (CPX) is a diagnostic tool used to detect serial changes in exercise capacity, and it is of particular benefit for patients with chronic HF to assess peak oxygen uptake (peak VO_2) and minute ventilation/carbon dioxide production (VE/VCO_2) slope since those parameters have functioned as predictors for overall mortality or determinants of risk stratification for such individuals [5–9].

Peak VO_2 seems to be accurate for evaluating the functional status of patients with chronic HF and non-ischemic dilated cardiomyopathy because the changes in echocardiographic variables assessed by dobutamine echocardiography are well correlated with peak VO_2 [10–13]. Meanwhile, the mechanisms of a high VE/VCO_2 slope are multifactorial. Abnormalities of ventilator reflex control, pulmonary hemodynamics and low cardiac index during exercise are all possible correlations [14,15], however, its direct association with inotropic effect on cardiac hemodynamics has remained unclear.

Therefore, this study aimed to investigate a potential association between CPX variables and the left ventricular (LV) responses during dobutamine stress testing (DST) in ambulatory patients with idiopathic dilated cardiomyopathy (IDCM).

* Corresponding author at: Department of Cardiology, Nagoya University Graduate School of Medicine, 65 Tsurumai-cho, Shouwa-ku, Nagoya 466-8560, Japan. Tel.: +81 52 744 2147; fax: +81 52 744 2211.
E-mail address: hirasiki@med.nagoya-u.ac.jp (A. Hirashiki).

0167-5273/$ – see front matter © 2011 Elsevier Ireland Ltd. All rights reserved.
doi:10.1016/j.ijcard.2011.05.065

2. Methods

2.1. Patients

We studied 38 consecutive IDCM patients at Nagoya University Hospital between December 2007 and December 2009. All patients were in sinus rhythm and on optimal pharmacological therapy, according to current guidelines for treatment of HF [16]. Ongoing medical therapy was kept unchanged at the time of the stress test. No patients had implantable cardioverter-defibrillators or pacemakers. Each patient was hospitalized for examination and underwent laboratory measurements, a pulmonary functional test, echocardiography, CPX, and cardiac catheterization. IDCM was defined on the basis of the presence of both a reduced LV ejection fraction (LVEF) (<50% as determined by contrast left ventriculography) and a dilated LV cavity, in the absence of coronary or valvular heart disease, hypertension, or secondary cardiac muscle disease caused by any known systemic condition, as determined by endomyocardial biopsy [17]. The study protocol was approved by the Ethics Review Board of Nagoya University School of Medicine (approval no. 359), and written informed consent was obtained from all study subjects. Blood samples were collected from the antecubital vein of fasted patients after they had rested for 20 min in the supine position. Routine blood biochemical analysis was performed in addition to measurement of the plasma brain natriuretic peptide (BNP), renin activity, aldosterone, epinephrine, and norepinephrine. The estimated glomerular filtration rate (GFR) was calculated by using an equation modified for Japanese: estimated GFR ($mL\,min^{-1}$) = 194 × (serum creatinine) $^{-1.094}$ × (age in years) $^{-0.287}$. To adjust for female sex, the equation was: estimated GFR female = estimated GFR × 0.739 [18].

2.2. Echocardiography

Standard M-mode and two-dimensional echocardiography, Doppler blood flow, and tissue Doppler imaging measurements were performed in agreement with the American Society of Echocardiography guidelines using the Vivid 7 system (Vivid 7, GE Healthcare, Milwaukee, WI, USA) [19]. Septal and posterior LV wall thicknesses were obtained from the parasternal long-axis view. The LV end-diastolic and end-systolic volumes were obtained from 4 apical and 2 chamber views [20]. The LVEF was calculated from 2-dimensional apical images according to the formula of modified Simpson's method. Pulse-wave Doppler echocardiography was used to assess mitral peak early (E) and late wave flow velocity and E-wave deceleration time. The tissue Doppler imaging wave sample of the mitral annulus was obtained from the septal side of the apical 4-chamber view. Analysis was performed for the early (Ea) diastolic peak velocity. The ratio of early transmitral flow velocity to early diastolic mitral annular velocity (E/Ea) was taken as an estimate of LV filling pressure [21].

2.3. CPX procedure and data collection

Each patient underwent CPX at a progressively increasing work rate to maximum tolerance on a cycle ergometer. The test protocol was in accordance with the recommendations of the American Thoracic Society and American College of Chest Physicians [22]. The oxygen and carbon dioxide sensors were calibrated before each test using gasses with known oxygen, nitrogen, and carbon dioxide concentrations. The flow sensor was also calibrated before each test using a 3-L syringe. All patients started at 10 W for 3 min warm-up, followed by a 10 W/min ramp increment protocol up to the termination criteria. Test termination criteria consisted of patient request, volitional fatigue, ventricular tachycardia, ≥2 mm of horizontal or downsloping ST segment depression, or a drop in systolic blood pressure ≥20 mm Hg during exercise. A qualified exercise physiologist conducted each test with physician supervision. A 12-lead electrocardiogram was monitored continuously, and blood pressure was measured every minute during exercise and throughout the recovery period. Respiratory gas exchange variables, including VO_2, VCO_2, and VE, were acquired continuously throughout the exercise testing using an Ergospirometry Oxycon Pro (Care Fusion; Sun Diego, CA, USA), and the gas-exchange data were obtained breath-by-breath. Peak VO_2 was expressed as the highest 30-second average value obtained during the last stage of the exercise test, and the peak respiratory exchange ratio was the highest 30-second averaged value during the last stage of the test. The VE/VCO_2 slope was determined by using linear regression analysis of VE and VCO_2 obtained during exercise [23]. The ventilatory threshold was determined in all patients by the classical method [24,25].

2.4. Cardiac catheterization and DST

All patients initially underwent routine diagnostic left and right heart catheterization. A 6-F fluid-filled pigtail catheter with a high-fidelity micromanometer (CA-61000-PLB Pressure-tip Catheter, CD Leycom, Zoetermeer, The Netherlands) was placed in the LV cavity for measurement of LV pressure. We evaluated the maximum first derivative of LV pressure (LV dP/dt_{max}) as an index of LV contractility, as previously described [26]. After collection of baseline hemodynamic data, dobutamine was infused intravenously at incremental doses of 5, 10, and 15 $\mu g\,kg^{-1}\,min^{-1}$, and hemodynamic measurements were made at the end of each 5-minute infusion period. In addition, we calculated ΔLV dP/dt_{max} as an index of myocardial contractile reserve [27]. ΔLV dP/dt_{max} was defined as the percentage increase in LV dP/dt_{max} induced by dobutamine, and this index was defined on the basis of the formula ΔLV dP/dt_{max} (x) (%) = [LV dP/dt_{max} (x) − LV dP/dt_{max} (baseline)]/LV dP/dt_{max} (baseline), where x = the dose of dobutamine ($\mu g\,kg^{-1}\,min^{-1}$).

2.5. Statistical analysis

Data are presented as means ± standard deviation. All statistical analyses were performed with the SPSS 17.0 software package (SPSS Inc., Chicago, IL, USA). To investigate the association between myocardial contractile reserve measured by DST and CPX variables, the relationship between echocardiographic index, hemodynamic parameters or biomarkers, and CPX variables was analyzed by using correlation coefficients and a linear regression analysis. As for the differences of measurements between two groups, normally distributed variables were compared by the Student's t test and non-normally distributed variables by the Mann–Whitney U test. Differences between three groups were analyzed by a two-way ANOVA followed by Turkey's post hoc test. Four major factors used widely in clinical practice — the plasma BNP level (biomarker), E/Ea ratio (LV diastolic performance), LVEF (LV systolic performance), and ΔLV dP/dt_{max} (10) — were used in a multivariate regression analysis to determine independent factors of peak VO_2 and VE/VCO_2 slope. A p-value of <0.05 was considered statistically significant.

3. Results

3.1. Baseline clinical characteristics

Baseline clinical characteristics of the patients are shown in Table 1. The mean age was 51.3 years old, and 92% of patients had mild symptoms, classified as New York Heart Association functional class I or II. Twenty-one (55%) patients had been treated with β-blockers. No patients had abnormal respiratory function. The peak VO_2 was 18.6 ± 5.2 $mL\,kg^{-1}\,min^{-1}$ and the VE/VCO_2 slope was 32.3 ± 10.8. The heart rate at baseline and peak exercise was 85.9 ± 16.1 and 131.1 ± 22.4 bpm, respectively. The mean LVEF measured by left ventriculography was 32.5%. There were no patients with severe pulmonary hypertension.

3.2. Hemodynamic responses by DST

Hemodynamic responses to intravenous dobutamine infusion are shown in Table 2. No complications occurred in any of the study subjects during the dobutamine stress protocol. The heart rate, LV systolic pressure and LV dP/dt_{max} were increased as the dose of dobutamine was increased. Contractile response (ΔLV dP/dt_{max}) increased significantly as the dose of dobutamine was increased (Fig. 1). There were no significant differences in LV dP/dt_{max} (5), LV dP/dt_{max} (10) between treatment groups with or without ß-blocker, whereas LV dP/dt_{max} (15) was only significantly lower in the ß-blocker (+) group than in the ß-blocker (−) group (Table 3). We observed that there were also no significant differences in all ΔLV dP/dt_{max} between two groups, even though it was increased as the dose of dobutamine was increased.

3.3. Myocardial contractile reserve and CPX parameters

The correlations between patient characteristics, biomarkers, echocardiographic data, or hemodynamic parameters and peak VO_2 or VE/VCO_2 slope are shown in Table 4. The plasma BNP level and E/Ea ratio were significantly correlated with peak VO_2 ($r = -0.538$, $r = -0.390$, respectively). The plasma BNP level was also correlated with VE/VCO_2 slope ($r = 0.764$). However, LVEF was not significantly correlated with peak VO_2 and VE/VCO_2 slope. Whereas the LV dP/dt_{max} at baseline was not significantly correlated with peak VO_2 ($r = 0.286$, $p = 0.081$), the LV dP/dt_{max} under the dobutamine infusion was significantly correlated with peak VO_2 (LV dP/dt_{max} (5); $r = 0.339$, LV dP/dt_{max} (10); $r = 0.428$, LV dP/dt_{max} (15); $r = 0.490$, respectively). In addition, the ΔLV dP/dt_{max} was significantly correlated with peak VO_2, and the correlation became more pronounced as the dose of dobutamine was increased (ΔLV dP/dt_{max} (5); $r = 0.329$, ΔLV dP/dt_{max} (10); $r = 0.508$, ΔLV dP/dt_{max} (15); $r = 0.601$, respectively) (Fig. 2). In contrast, no significant correlation between ΔLV dP/dt_{max} and

Table 1
Baseline clinical characteristics (n = 38).

Age (yrs)	51.3 ± 13.1
Gender, male/female	25/13
Body mass index (kg m^{-2})	23.5 ± 4.4
NYHA functional class (I/II/III/IV)	(23/12/3/0)
Medication, n (%)	
β-blockers	21 (55)
ACE inhibitors	6 (16)
ARBs	
19 (50)	
Diuretics	21 (55)
Spironoractone	17 (43)
Statins	
5 (13)	
Laboratory measurements	
Hemoglobin (g dL^{-1})	13.5 ± 1.6
Estimated GFR (mL min^{-1})	68.4 ± 28.3
Plasma norepinephrine (ng mL^{-1})	0.569 ± 0.311
Plasma BNP (pg mL^{-1})	203.1 ± 225.5
Respiratory function	
FVC% predicted	104.0 ± 15.0
FEV1% predicted	79.3 ± 6.8
DL_{CO} (mL min^{-1} mm Hg^{-1})	20.7 ± 6.6
Echocardiography	
LV end-diastolic diameter (mm)	63.6 ± 9.2
LV end-systolic diameter (mm)	53.5 ± 10.7
Left atrial diameter (mm)	40.9 ± 8.5
E/A ratio	1.3 ± 0.8
Deceleration time (ms)	203.8 ± 60.8
E/Ea ratio	15.4 ± 8.8
MR (none or trivial/mild/moderate/severe)	(22/10/3/3)
CPX variables	
Baseline heart rate (beats min^{-1})	85.9 ± 16.1
Peak heart rate (beats min^{-1})	131.1 ± 22.4
Baseline systolic blood pressure (mm Hg)	118.4 ± 23.9
Peak systolic blood pressure (mm Hg)	159.3 ± 45.2
Peak VO_2 (mL kg^{-1} min^{-1})	18.6 ± 5.2
VE/VCO_2 slope	32.3 ± 10.8
$\Delta VO_2/\Delta WR$ (mL min^{-1} W^{-1})	9.1 ± 2.9
Peak RER	1.08 ± 0.09
Cardiac catheterization	
LV ejection fraction (%)	32.5 ± 10.4
LV end-diastolic volume (mL)	254.3 ± 92.7
LV end-systolic volume (mL)	183.2 ± 87.4
PAWP (mm Hg)	11.8 ± 5.8
Systolic PA pressure (mm Hg)	25.9 ± 9.3
Cardiac index (L min^{-1} m^{-2})	2.78 ± 0.52
LV end-diastolic pressure (mm Hg)	15.2 ± 8.7

Data are means ± SD.
NYHA = New York Heart Association; ACE = angiotensin-converting enzyme; ARB = angiotensin II receptor blocker; GFR = glomerular filtration rate; BNP = brain natriuretic peptide; FVC = forced vital capacity; FEV1% = forced expiratory volume in 1 second as percent of FVC; DLco = diffusing capacity for carbon monoxide; LV = left ventricular; E/Ea ratio = ratio of early transmitral flow velocity to early diastolic mitral annular velocity; MR = mitral regurgitation; CPX = cardiopulmonary exercise testing; peak VO_2 = peak oxygen uptake; VE/VCO_2 slope = the minute ventilation/carbon dioxide production; $\Delta VO_2/\Delta WR$ = the ratio of the increase in VO_2 to the increase in work rate; RER = respiratory exchange ratio; PAWP = pulmonary arterial wedge pressure; PA = pulmonary artery.

VE/VCO_2 slope was observed (ΔLV dP/dt_{max} (5); p = 0.257, ΔLV dP/dt_{max} (10); p = 0.161, ΔLV dP/dt_{max} (15); p = 0.085, respectively). Multivariate regression analysis revealed that ΔLV dP/dt_{max} (10) and plasma BNP level were independently correlated with peak VO_2 (p = 0.011, p = 0.001, respectively) (Table 5). We observed that plasma BNP levels was only independently significant correlated with VE/VCO_2 slope, whereas ΔLV dP/dt_{max} (10) was not significantly correlated with VE/VCO_2 slope (p = 0.708).

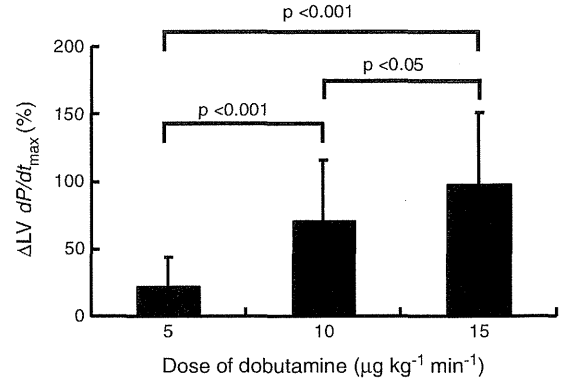

Fig. 1. Contractile response to dobutamine stress testing. Left ventricular hemodynamic response of 38 patients to dobutamine stress testing. Data are shown as means ± SD. ΔLV dP/dt_{max} increased significantly as the dose of dobutamine was increased.

4. Discussion

In the present study, we investigated the association between LV response to dobutamine and CPX variables to examine our hypothesis that myocardial contractile reserve correlates closely with exercise functional capacity. Our results showed that the myocardial contractile reserve measured by DST was strongly correlated with peak VO_2 as the dose of dobutamine was increased, whereas it was not correlated with VE/VCO_2 slope. In addition, the contractile reserve by DST was independently correlated with peak VO_2. These findings suggest that only peak VO_2, and not VE/VCO_2 slope, reflects myocardial contractile reserve in patients with IDCM. To our knowledge, this investigation is the first to report the relationship between myocardial contractile reserve as assessed by DST using directly measured LV pressure and CPX variables — especially the 2 major prognostic parameters, peak VO_2 and VE/VCO_2 slope — in patients with IDCM.

Peak VO_2 and VE/VCO_2 slope are 2 major powerful predictors of mortality in HF patients with severe systolic LV dysfunction [9], but a dissociation between peak VO_2 and VE/VCO_2 slope is occasionally seen in patients with HF. Peak VO_2, measured at the end of the test, is widely used as the diagnostic and prognostic surrogate marker in patients with HF [8]. However, the end point of an exercise test is greatly influenced by motivation on the part of the patients and the testing personnel [28]. In addition, cardiac output cannot be accurately estimated from CPX, largely because VO_2 is influenced by numerous central and peripheral factors [29]. On the other hand, a growing body of studies over last decade has demonstrated that VE/VCO_2 slope more powerfully predicts mortality or hospitalization than peak VO_2 among HF patients [30]. VE/VCO_2 slope is influenced not only cardiac function but also respiratory physiological deregulation such as ergoreflex or chemoreflex sensitivity, and inversely correlated with exercise tolerance in chronic HF [28].

Table 2
Hemodynamic response to intravenous dobutamine infusion.

Parameter	Baseline	Dobutamine (5 μg kg^{-1} min^{-1})	Dobutamine (10 μg kg^{-1} min^{-1})	Dobutamine (15 μg kg^{-1} min^{-1})
Heart rate (beats min^{-1})	74.0 ± 14.5	77.0 ± 16.3	88.8 ± 20.9	101.1 ± 23.8
LVSP (mm Hg)	122.0 ± 25.8	127.7 ± 31.4	139.5 ± 42.2	136.7 ± 35.4
LV dP/dt_{max} (mm Hg s^{-1})	1079.8 ± 299.4	1353.3 ± 583.8	1920.2 ± 891.3	2203.8 ± 994.1

Data are means ± SD.
LVSP = left ventricular systolic pressure; LV dP/dt_{max} = maximal first derivative of left ventricular pressure.

Table 3
Comparison of hemodynamic response by DST between treatment groups with or without ß-blocker.

Parameter	ß-blocker (−)(n = 17)	ß-blocker (+)(n = 21)	p-value
Heart rate (beats min^{-1})			
Baseline	79.5 ± 15.1	69.5 ± 12.8	0.04
Dobutamine (5 μg kg^{-1} min^{-1})	85.8 ± 13.9	69.9 ± 14.8	0.002
Dobutamine (10 μg kg^{-1} min^{-1})	103.3 ± 17.0	77.3 ± 16.1	0.00004
Dobutamine (15 μg kg^{-1} min^{-1})	118.6 ± 16.6	86.4 ± 18.5	0.000006
LVSP (mm Hg)			
Baseline	123.0 ± 27.0	121.1 ± 25.5	0.83
Dobutamine (5 μg kg^{-1} min^{-1})	130.1 ± 34.0	125.7 ± 29.9	0.68
Dobutamine (10 μg kg^{-1} min^{-1})	133.9 ± 33.2	144.0 ± 48.6	0.48
Dobutamine (15 μg kg^{-1} min^{-1})	132.7 ± 31.6	140.1 ± 38.8	0.55
LV dP/dt_{max} (mm Hg s^{-1})			
Baseline	159.2 ± 278.0	1019.3 ± 307.5	0.16
Dobutamine (5 μg kg^{-1} min^{-1})	1448.9 ± 624.8	1189.8 ± 357.1	0.13
Dobutamine (10 μg kg^{-1} min^{-1})	2073.3 ± 806.6	1646.6 ± 597.2	0.08
Dobutamine (15 μg kg^{-1} min^{-1})	2452.9 ± 1056.0	1851.5 ± 575.3	0.04
ΔLV dP/dt_{max}			
Dobutamine (5 μg kg^{-1} min^{-1})	26.2 ± 34.8	14.5 ± 9.4	0.16
Dobutamine (10 μg kg^{-1} min^{-1})	79.1 ± 45.2	56.4 ± 24.5	0.06
Dobutamine (15 μg kg^{-1} min^{-1})	110.1 ± 58.2	82.5 ± 34.5	0.09

Data are means ± SD.
DST = dobutamine stress testing; LVSP = left ventricular systolic pressure; LV dP/dt_{max} = maximal first derivative of left ventricular pressure; ΔLV dP/dt_{max} = the percentage increase in LV dP/dt_{max} induced by dobutamine.

Table 4
Correlation between ecocardiographic index, hymodynamic parameters or biomarkers and CPX variables.

	Peak VO_2		VE/VCO_2 slope	
	r	p-value	r	p-value
Age	0.076	0.651	0.070	0.677
Body mass index	−0.059	0.726	−0.439	0.006
Laboratory measurement				
Hemoglobin	0.203	0.222	−0.396	0.014
Estimated GFR	0.109	0.515	−0.112	0.504
Norepinephrine	−0.094	0.576	−0.230	0.165
Plasma BNP	−0.538	<0.001	0.764	<0.001
Echocardiography				
LV end-diastolic diameter	−0.306	0.062	0.268	0.104
LV end-systolic diameter	−0.297	0.070	0.332	0.042
Left atrial diameter	−0.314	0.055	0.332	0.041
E/A ratio	−0.275	0.094	0.750	<0.001
Decerelation time	0.114	0.496	−0.218	0.188
E/Ea ratio	−0.390	0.016	0.255	0.122
CPX variables				
Baseline heart rate	0.079	0.637	−0.291	0.0762
Peak heart rate	0.507	0.001	−0.491	0.002
Baseline systolic blood pressure	0.132	0.428	−0.536	<0.001
Peak systolic blood pressure	0.470	0.003	−0.646	<0.001
Cardiac catheterization				
LV ejection fraction	0.211	0.204	−0.277	0.092
LV end-diastolic pressure	−0.097	0.564	0.304	0.063
LV end-diastolic volume	−0.070	0.677	0.419	0.009
Cardiac index	0.347	0.033	−0.493	0.002
PAWP	−0.342	0.036	0.276	0.093
Systolic PA pressure	−0.353	0.030	0.364	0.025
LV dP/dt_{max} at baseline	0.286	0.081	−0.557	<0.001
LV dP/dt_{max} (5 μg kg^{-1} min^{-1})	0.339	0.037	−0.388	0.016
LV dP/dt_{max} (10 μg kg^{-1} min^{-1})	0.428	0.007	−0.355	0.029
LV dP/dt_{max} (15 μg kg^{-1} min^{-1})	0.490	0.002	−0.395	0.014

CPX = cardiopulmonary exercise testing; peak VO_2 = peak oxygen uptake; VE/VCO_2 slope = the minute ventilation/carbon dioxide production; GFR = glomerular filtration rate; BNP = brain natriuretic peptide; LV = left ventricular; E/Ea ratio = ratio of early transmitral flow velocity to early diastolic mitral annular velocity; PAWP = pulmonary arterial wedge pressure; PA = pulmonary artery; LV dP/dt_{max} = maximal first derivative of left ventricular pressure.

Dobutamine is a direct β-agonist that has been used to evaluate myocardial contractile reserve in chronic HF [31]. Few studies have evaluated the adrenergic contractile response to dobutamine infusion by measurement of the increase in LV dP/dt_{max} in patients with non-ischemic LV systolic dysfunction [32,33]. Several studies based on dobutamine stress echocardiography have shown a relationship between prognosis and adrenergic myocardial contractile reserve, as determined by measurement of LV systolic function indices such as LVEF or cardiac output [10,34]. However, many investigations which reported DST were measured by echocardiography [10,11]; here, we more accurately evaluated dobutamine response by measuring using catheterization with a high-fidelity micromanometer.

Decreased response to dobutamine infusion is a marker of the pathological status of myocardial damage and is closely associated with impaired peak VO_2 [27]. In the present study, peak VO_2 was significantly correlated with the absolute value of LV dP/dt_{max} and more strongly correlated with ΔLV dP/dt_{max}. Peak VO_2 was also independently correlated with ΔLV dP/dt_{max} and plasma BNP level. On the other hand, VE/VCO_2 slope was not correlated with ΔLV dP/dt_{max}. Because the percentage increase in LV dP/dt_{max} induced by dobutamine is especially unaffected by factors such as peripheral ergoreceptor activation, hyperventilation, and LV dP/dt_{max} at baseline, it is thought to be a useful and direct assessment of myocardial contractile reserve. Therefore, the results of this study suggest that myocardial contractile reserve may be strong determinant for peak VO_2, but not VE/VCO_2 slope in our study population. Furthermore, VE/VCO_2 slope was strongly correlated with plasma BNP level. The abnormal ventilatory response to exercise seems to be related to sympathetic activation, renin–angiotensin system [35] and ergoreflex activation [36] rather than to myocardial contractile reserve.

Our group reported previously that DST is a useful diagnostic tool for identifying reduced adrenergic contractile reserve related to altered myocardial expression of the β_1-adrenergic receptor and Ca^{2+}-handling mRNA level, even in asymptomatic or mildly symptomatic patients with IDCM [27]. A direct relationship of the degree of β_1-receptor down-regulation to peak VO_2 was also found in patients with IDCM [37]. These results suggest that decreased peak VO_2 is potentially related to impaired Ca^{2+}-handling or β_1-adrenergic receptor in patients with IDCM.

Myocardial contractile reserve, as determined by dobutamine stress echocardiography, predicts improvement in LVEF with β-blocker therapy [29]. In the absence of contractile reserve (i.e., when myocytes have been supplanted by replacement fibrosis because of cell death and interstitial remodeling), ventricular function cannot be improved by this biological mechanism because there are not enough contractile units. Contractile reserve itself appears to improve after LVEF has increased with β-blocker therapy. Thus, the benefit of β-blockade in HF patients is related not only to improvement in resting ventricular function but also to improved contractile reserve and the ability to respond to stress, likely to be found during exercise. However, we did not measure contractile reserve after β-blocker therapy. Higher peak VO_2 might indicate higher contractile reserve, and therefore a better potential response to β-blocker therapy and improved prognosis.

CPX is a useful tool for assessment of exercise tolerance and therapeutic effects in patients with HF, and accurate and repetitive measurements are available to the clinician at a reasonable cost. Indeed,

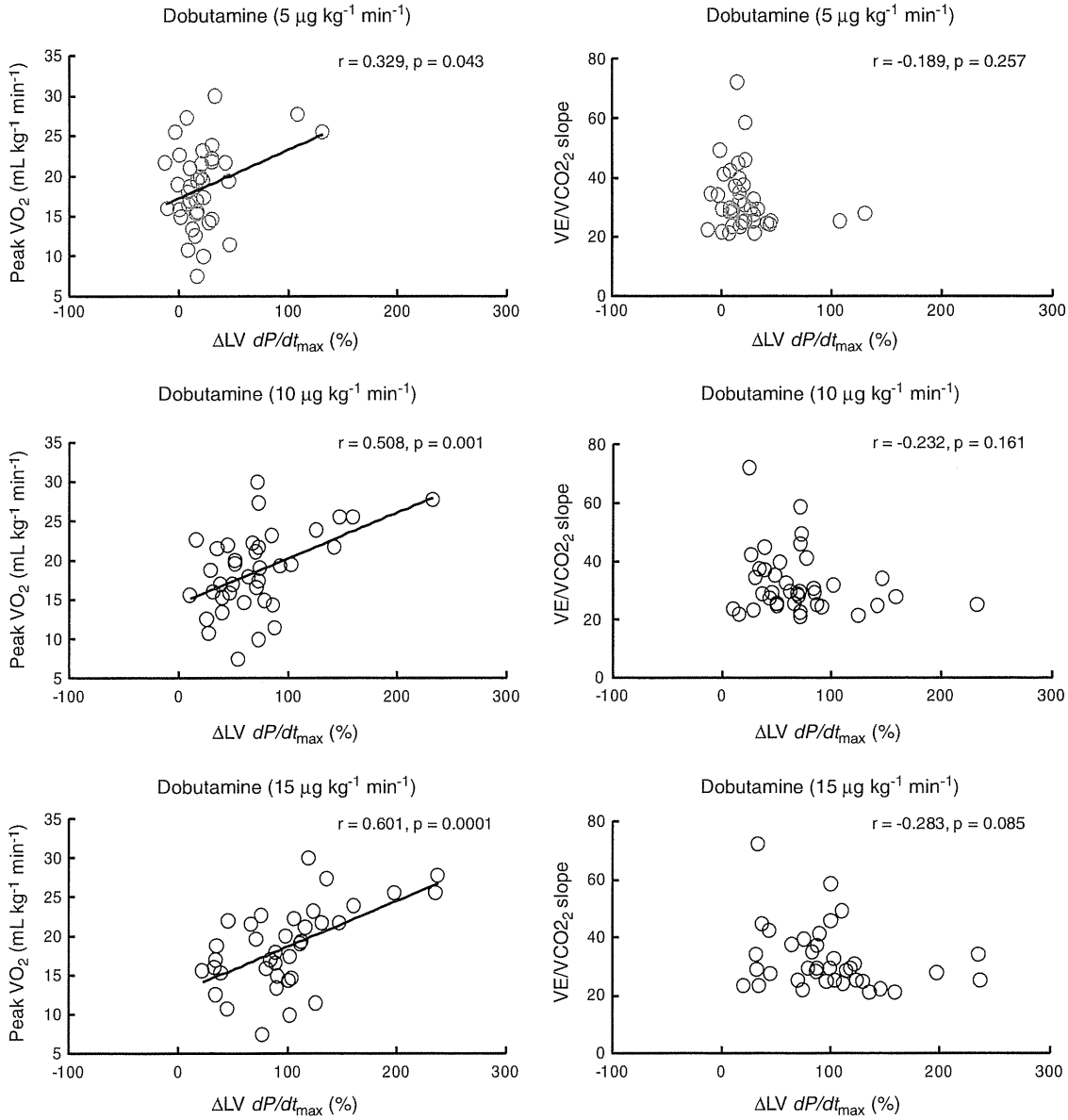

Fig. 2. Correlation between myocardial contractile reserve and peak VO_2, VE/VCO_2 slope. $\Delta LV\ dP/dt_{max}$ was significantly correlated with peak VO_2, and the correlation became more pronounced as the dose of dobutamine was increased. In contrast, no significant inverse correlation between $\Delta LV\ dP/dt_{max}$ and VE/VCO_2 slope was apparent, even at the maximum dose of dobutamine. $\Delta LV\ dP/dt_{max}$ is the percentage increase in LV dP/dt_{max} induced by dobutamine, and this index was defined on the basis of the formula: $\Delta LV\ dP/dt_{max}$ (x) (%) = [LV dP/dt_{max} (x) − LV dP/dt_{max} (baseline)] / LV dP/dt_{max} (baseline), where x = the dose of dobutamine ($\mu g\ kg^{-1}\ min^{-1}$).

especially for the observation of cardiac deterioration in patients with known IDCM, peak VO_2 possibly provide meaningful clinical information as a surrogate for cardiac reserve. Given the results of this study, peak VO_2 can represent myocardial contractile reserve, indicating that preserved systolic contractile reserve may be a feature in relatively mild degree of heart failure, in ambulatory patients with IDCM.

There are several limitations in our study. First, this study was performed in a small number of patients. Second, as regards to medication,

Table 5
Multivariate regression analysis of CPX variables.

Parameter	Peak VO_2			VE/VCO_2 slope		
	β	(95% CI)	p-value	β	(95% CI)	p-value
$\Delta LV\ dP/dt_{max}$ ($10\ \mu g\ kg^{-1}\ min^{-1}$)	0.430	(0.012–0.086)	0.011	0.052	(−0.054–0.079)	0.708
BNP	−0.421	(−0.017–−0.002)	0.010	0.813	(0.026–0.052)	<0.001
LVEF	−0.251	(−0.288–0.039)	0.131	0.064	(−0.228–0.362)	0.648
E/Ea ratio	−0.183	(−0.272–0.059)	0.201	0.001	(−0.299–0.301)	0.995

CPX = cardiopulmonary exercise testing; peak VO_2 = peak oxygen uptake; VE/VCO_2 slope = minute ventilation/carbon dioxide production; LV dP/dt_{max} = maximum first derivative of left ventricular pressure; $\Delta LV\ dP/dt_{max}$ = percentage increase in LV dP/dt_{max} induced by dobutamine; BNP = brain natriuretic peptide; LVEF = left ventricular ejection fraction; E/Ea ratio = ratio of early transmitral flow velocity to early diastolic mitral annular velocity; CI = confidence interval.

especially patients on β-blocking agents, therapy was kept unchanged. This may have resulted in some false-negative results in DST. However, the optimum dose of dobutamine to assess contractility is not defined, and it did not appear ethical to withhold a lifesaving therapy. Third, the assessment of peripheral factors was not checked. The patients in the present study had a mean of peak VO_2 of 18.6 mL kg^{-1} min^{-1}, which was relatively preserved exercise tolerance in IDCM patients. Because all subjects in this study were ambulatory and in stable condition, with normal respiratory function and relatively mild symptoms, the influence of lung and peripheral factors on VO_2 might be minimum.

In conclusion, based on DST findings, we suggest that peak VO_2, but not VE/VCO_2 slope, reflects myocardial contractile reserve. The findings of our study may provide evidence to differentiate pathophysiological insights between peak VO_2 and VE/VCO_2 slope, major prognostic CPX parameters. Further research could be designed to observe time course of deterioration of cardiac reserve by peak VO_2 as a surrogate marker. Further studies with larger numbers of patients, including those with more severe HF symptoms, are needed before our results can be applied more generally to IDCM patients with HF.

Funding

The work was supported in part by the Ministry of Education, Culture, Sports, Science and Technology of Japan [grant number 21790716 to A.H.].

Acknowledgements

The authors of this manuscript have certified that they comply with the Principles of Ethical Publishing in the International Journal of Cardiology.

References

[1] Jessup M, Brozena S. Heart failure. N Engl J Med 2003;348:2007–18.
[2] Myers J, Prakash M, Froelicher V, Do D, Partington S, Atwood JE. Exercise capacity and mortality among men referred for exercise testing. N Engl J Med 2002;346:793–801.
[3] Wroblewski H, Kastrup J, Mortensen SA, Haunso S. Abnormal baroreceptor-mediated vasodilation of the peripheral circulation in congestive heart failure secondary to idiopathic dilated cardiomyopathy. Circulation 1993;87:849–56.
[4] McBride BF, White CM. Anemia management in heart failure: a thick review of thin data. Pharmacotherapy 2004;24:757–67.
[5] O'Neill JO, Young JB, Pothier CE, Lauer MS. Peak oxygen consumption as a predictor of death in patients with heart failure receiving beta-blockers. Circulation 2005;111:2313–8.
[6] Guazzi M, Myers J, Peberdy MA, et al. Echocardiography with Tissue Doppler Imaging and cardiopulmonary exercise testing in patients with heart failure: a correlative and prognostic analysis. Int J Cardiol 2010;143:323–9.
[7] Corra U, Mezzani A, Bosimini E, Scapellato F, Imparato A, Giannuzzi P. Ventilatory response to exercise improves risk stratification in patients with chronic heart failure and intermediate functional capacity. Am Heart J 2002;143:418–26.
[8] Dickstein K, Cohen-Solal A, Filippatos G, et al. ESC Guidelines for the diagnosis and treatment of acute and chronic heart failure 2008: the Task Force for the Diagnosis and Treatment of Acute and Chronic Heart Failure 2008 of the European Society of Cardiology. Developed in collaboration with the Heart Failure Association of the ESC (HFA) and endorsed by the European Society of Intensive Care Medicine (ESICM). Eur Heart J 2008;29:2388–442.
[9] Jessup M, Abraham WT, Casey DE, et al. 2009 focused update: ACCF/AHA Guidelines for the Diagnosis and Management of Heart Failure in Adults: a report of the American College of Cardiology Foundation/American Heart Association Task Force on Practice Guidelines: developed in collaboration with the International Society for Heart and Lung Transplantation. Circulation 2009;119:1977–2016.
[10] Scrutinio D, Napoli V, Passantino A, Ricci A, Lagioia R, Rizzon P. Low-dose dobutamine responsiveness in idiopathic dilated cardiomyopathy: relation to exercise capacity and clinical outcome. Eur Heart J 2000;21:927–34.
[11] Paraskevaidis IA, Adamopoulos S, Kremastinos DT. Dobutamine echocardiographic study in patients with nonischemic dilated cardiomyopathy and prognostically borderline values of peak exercise oxygen consumption: 18-month follow-up study. J Am Coll Cardiol 2001;37:1685–91.
[12] Natali R, Lotrionte M, Marchese N, et al. Prediction of functional capacity by low-dose dobutamine stress echocardiography in chronic heart failure. Minerva Cardioangiol 2008;56:277–85.
[13] Paraskevaidis IA, Tsiapras DP, Adamopoulos S, Kremastinos DT. Assessment of the functional status of heart failure in non ischemic dilated cardiomyopathy: an echo-dobutamine study. Cardiovasc Res 1999;43:58–66.
[14] Chua TP, Clark AL, Amadi AA, Coats AJ. Relation between chemosensitivity and the ventilatory response to exercise in chronic heart failure. J Am Coll Cardiol 1996;27:650–7.
[15] Griffin BP, Shah PK, Ferguson J, Rubin SA. Incremental prognostic value of exercise hemodynamic variables in chronic congestive heart failure secondary to coronary artery disease or to dilated cardiomyopathy. Am J Cardiol 1991;67:848–53.
[16] Hunt SA, Abraham WT, Chin MH, et al. ACC/AHA 2005 Guideline Update for the Diagnosis and Management of Chronic Heart Failure in the Adult: a report of the American College of Cardiology/American Heart Association Task Force on Practice Guidelines (Writing Committee to Update the 2001 Guidelines for the Evaluation and Management of Heart Failure): developed in collaboration with the American College of Chest Physicians and the International Society for Heart and Lung Transplantation: endorsed by the Heart Rhythm Society. Circulation 2005;112:e154–235.
[17] Richardson P, McKenna W, Bristow M, et al. Report of the 1995 World Health Organization/International Society and Federation of Cardiology Task Force on the Definition and Classification of cardiomyopathies. Circulation 1996;93:841–2.
[18] Matsuo S, Imai E, Horio M, et al. Revised equations for estimated GFR from serum creatinine in Japan. Am J Kidney Dis 2009;53:982–92.
[19] Cheitlin MD, Armstrong WF, Aurigemma GP, et al. ACC/AHA/ASE 2003 guideline update for the clinical application of echocardiography—summary article: a report of the American College of Cardiology/American Heart Association Task Force on Practice Guidelines (ACC/AHA/ASE Committee to Update the 1997 Guidelines for the Clinical Application of Echocardiography). J Am Coll Cardiol 2003;42:954–70.
[20] Lang RM, Bierig M, Devereux RB, et al. Recommendations for chamber quantification: a report from the American Society of Echocardiography's Guidelines and Standards Committee and the Chamber Quantification Writing Group, developed in conjunction with the European Association of Echocardiography, a branch of the European Society of Cardiology. J Am Soc Echocardiogr 2005;18:1440–63.
[21] Ommen SR, Nishimura RA, Appleton CP, et al. Clinical utility of Doppler echocardiography and tissue Doppler imaging in the estimation of left ventricular filling pressures: a comparative simultaneous Doppler-catheterization study. Circulation 2000;102:1788–94.
[22] ATS/ACCP. Statement on cardiopulmonary exercise testing. Am J Respir Crit Care Med 2003;167:211–77.
[23] Bard RL, Gillespie BW, Clarke NS, Egan TG, Nicklas JM. Determining the best ventilatory efficiency measure to predict mortality in patients with heart failure. J Heart Lung Transplant 2006;25:589–95.
[24] Wasserman K, Whipp BJ, Koyl SN, Beaver WL. Anaerobic threshold and respiratory gas exchange during exercise. J Appl Physiol 1973;35:236–43.
[25] Wasserman K, Beaver WL, Whipp BJ. Gas exchange theory and the lactic acidosis (anaerobic) threshold. Circulation 1990;81:II14–30.
[26] Somura F, Izawa H, Iwase M, et al. Reduced myocardial sarcoplasmic reticulum Ca(2+)-ATPase mRNA expression and biphasic force-frequency relations in patients with hypertrophic cardiomyopathy. Circulation 2001;104:658–63.
[27] Kobayashi M, Izawa H, Cheng XW, et al. Dobutamine stress testing as a diagnostic tool for evaluation of myocardial contractile reserve in asymptomatic or mildly symptomatic patients with dilated cardiomyopathy. JACC Cardiovasc Imaging 2008;1:718–26.
[28] Piepoli M, Clark AL, Volterrani M, Adamopoulos S, Sleight P, Coats AJ. Contribution of muscle afferents to the hemodynamic, autonomic, and ventilatory responses to exercise in patients with chronic heart failure: effects of physical training. Circulation 1996;93:940–52.
[29] Eichhorn EJ, Grayburn PA, Mayer SA, et al. Myocardial contractile reserve by dobutamine stress echocardiography predicts improvement in ejection fraction with beta-blockade in patients with heart failure: the Beta-Blocker Evaluation of Survival Trial (BEST). Circulation 2003;108:2336–41.
[30] Chua TP, Ponikowski P, Harrington D, et al. Clinical correlates and prognostic significance of the ventilatory response to exercise in chronic heart failure. J Am Coll Cardiol 1997;29:1585–90.
[31] Leier CV, Unverferth DV. Drugs five years later. Dobutamine. Ann Intern Med 1983;99:490–6.
[32] Fowler MB, Laser JA, Hopkins GL, Minobe W, Bristow MR. Assessment of the beta-adrenergic receptor pathway in the intact failing human heart: progressive receptor down-regulation and subsensitivity to agonist response. Circulation 1986;74:1290–302.
[33] Dubois-Rande JL, Merlet P, Roudot F, et al. Beta-adrenergic contractile reserve as a predictor of clinical outcome in patients with idiopathic dilated cardiomyopathy. Am Heart J 1992;124:679–85.
[34] Naqvi TZ, Goel RK, Forrester JS, Siegel RJ. Myocardial contractile reserve on dobutamine echocardiography predicts late spontaneous improvement in cardiac function in patients with recent onset idiopathic dilated cardiomyopathy. J Am Coll Cardiol 1999;34:1537–44.
[35] Passino C, Poletti R, Bramanti F, Prontera C, Clerico A, Emdin M. Neuro-hormonal activation predicts ventilatory response to exercise and functional capacity in patients with heart failure. Eur J Heart Fail 2006;8:46–53.
[36] Ponikowski PP, Chua TP, Francis DP, Capucci A, Coats AJ, Piepoli MF. Muscle ergoreceptor overactivity reflects deterioration in clinical status and cardiorespiratory reflex control in chronic heart failure. Circulation 2001;104:2324–30.
[37] White M, Yanowitz F, Gilbert EM, et al. Role of beta-adrenergic receptor down-regulation in the peak exercise response in patients with heart failure due to idiopathic dilated cardiomyopathy. Am J Cardiol 1995;76:1271–6.